

Beyond- Λ CDM Cosmologies with Bayesian Neural Networks II: Massive Neutrinos, Baryonic Feedback, and the Theoretical Error

L. Thummel,^{1,2*} B. Bose,^{1,3} A. Pourtsidou,^{1,2} L. Lombriser⁴

¹*Institute for Astronomy, University of Edinburgh, Royal Observatory, Blackford Hill, Edinburgh, EH9 3HJ, UK*

²*Higgs Centre for Theoretical Physics, University of Edinburgh, James Clerk Maxwell Building, Edinburgh, EH9 3FD, UK*

³*Basic Research Community for Physics e.V., Mariannenstraße 89, Leipzig, Germany*

⁴*Département de Physique Théorique, Université de Genève, 1211 Genève 4, Switzerland*

Accepted XXX. Received YYY; in original form ZZZ

ABSTRACT

We study the capacity of Bayesian Neural Networks (BNNs) to detect new physics in the dark matter power spectrum. As in previous studies, the Bayesian Cosmological Network (BaCoN) classifies spectra into one of 5 classes: Λ CDM, $f(R)$, w CDM, Dvali-Gabadaze-Porrati (DGP) gravity and a “random” class, with this work extending it to include the effects of massive neutrinos and baryonic feedback. We further develop the treatment of theoretical errors in BaCoN-II, investigating several approaches and identifying the one that best allows the trained network to generalise to other power spectrum modelling prescriptions. In particular, we compare power spectra data produced by `EuclidEmulator2`, `HMcode` and `halofit`, all supplemented with the halo model reaction to model beyond- Λ CDM physics. We investigate BNN-classifiers trained on these sets of spectra, adding in Stage-IV survey noise and various theoretical error models. Using our optimal theoretical error model, our fiducial classifier achieves a total classification accuracy of $\sim 95\%$ when it is trained on `EuclidEmulator2`-based spectra with modification parameters drawn from a Gaussian distribution centred around Λ CDM ($f(R)$: $\sigma_{fR0} = 10^{-5.5}$, DGP: $\sigma_{rc} = 0.173$, w CDM: $\sigma_{w0} = 0.097$, $\sigma_{wa} = 0.32$). This strengthens the promise of this method to glean the maximal amount of unbiased gravitational and cosmological information from forthcoming Stage-IV galaxy surveys.

Key words: large-scale structure of Universe – dark energy – cosmology: theory – software: data analysis

1 INTRODUCTION

1.1 Cosmology

The concordance model of cosmology (Λ CDM) remains largely consistent with the vast amount of cosmological data produced during the last three decades (see [Huterer & Shafer 2018](#), for example). The model is largely characterised by the two ‘dark’ cosmological components that dominate our present Universe: dark energy in the form of a cosmological constant (Λ) and cold dark matter (CDM). These cosmological energy densities are needed for the theory to match a wide range of data sets such as the cosmic microwave background (CMB) measurements ([Aghanim et al. 2020a](#)) and cosmic large scale structure (LSS) measurements ([Anderson et al. 2013](#); [Song et al. 2015](#); [Beutler et al. 2017](#); [Hilbrandt et al. 2017](#); [Heymans et al. 2021](#); [Abbott et al. 2020](#); [Gatti et al. 2021](#)). Dark matter is also needed to match smaller astrophysical and cluster scale data ([Clowe et al. 2006](#); [Corbelli & Salucci 2000](#); [Allen et al. 2011](#)). The nature of these components, as well as their links to other fundamental physical problems, such as the cosmological constant problem (see [Bernardo et al. 2023](#), for a recent review), have been the focus of intense investigation over the past 25 years.

In this direction, many different theoretical ideas have been imag-

ined and tested (for example [Dvali et al. 2000](#); [Burgess 2004](#); [Brax & Valageas 2017](#)). Often these can be represented as a scalar tensor theory of gravity, or ‘modified gravity’ more generally ([Clifton et al. 2012](#)), or some non-trivial dark energy component ([Copeland et al. 2006](#)). Many of these model’s degrees of freedom have been well constrained by data or have exhibited theoretical or conceptual issues (see [Koyama 2016](#), for a review). Nevertheless, such characterisations of departures from Λ CDM and General Relativity (GR) should be tested by new data sets in order to guide future theoretical development.

An important anchor in such tests is that any new physics should be unobserved in our local part of the Universe. This instruction comes from the exquisite tests of GR (see [Will 2014](#), for a review) and various table-top experiments of modified gravity (see [Burrage 2019](#), for example). Thus, we must shut-off the effects of any additional degrees of freedom in the local Universe. Such theoretical mechanisms have been dubbed ‘screening mechanisms’ and are well studied in the context of modified gravity ([Brax et al. 2021](#)).

Other noteworthy observational constraints come from the large-scale data sets, including CMB and large scale structure measurements. These constraints have been placed on a wide range of possible departures from Λ CDM, particularly in the context of the Effective field theory of Dark Energy (EFTofDE) ([Gubitosi et al. 2013](#); [Salvatelli et al. 2016](#); [Perenon et al. 2019](#); [Noller 2020](#)), with statistical preference still generally given to Λ CDM. One is also instructed by

* E-mail: linus.thummel@ed.ac.uk

the measurement of incredibly consistent electromagnetic radiation and gravitational wave speeds (Lombriser & Taylor 2016; Abbott et al. 2017; Lombriser & Lima 2017; Creminelli & Vernizzi 2017; Ezquiaga & Zumalacárregui 2017; Baker et al. 2017; Sakstein & Jain 2017; Battye et al. 2018; de Rham & Melville 2018; Creminelli et al. 2018). Despite this, we must keep in mind the energy scales that these constraints probe which may have no bearing on the large scale gravitational or cosmological theory (see de Rham & Melville 2018, for example).

One major probe of new physics still left to be tapped is the smaller (nonlinear) scales of the large scale structure, which will be exquisitely measured by ongoing and forthcoming galaxy surveys such as Euclid (Laureijs et al. 2011; Amendola et al. 2018; Blanchard et al. 2020a), DESI (Levi et al. 2019), the Nancy Grace Roman Space Telescope (Akeson et al. 2019) and the Vera Rubin Observatory (LSST Dark Energy Science Collaboration 2012). At smaller scales we are benefiting from improved galaxy statistics and so measurement errors become much smaller. The extension of data analyses to the nonlinear regime can be achieved with accurate nonlinear prescriptions such as emulators of key quantities (Angulo et al. 2020; Knabenhans et al. 2021; Nishimichi et al. 2019; Donald-McCann et al. 2021; Kobayashi et al. 2020). This is generally only the case for consistency tests of Λ CDM, or particular extensions thereof (Winther et al. 2019; Arnold et al. 2021; Ramachandra et al. 2021).

In this direction, a theoretically general and accurate approach to the nonlinear regime for beyond- Λ CDM models was proposed in Cataneo et al. (2019, 2020); Bose et al. (2021), named the *halo model reaction*, with a general parametrisation for this framework further developed in Bose et al. (2022). The associated ReACT code (Bose et al. 2020, 2022, ) allows fast computations of beyond- Λ CDM corrections of cosmological matter density field correlations. Coupled with Λ CDM prescriptions for these correlations, one has a means of predicting these beyond- Λ CDM correlations in the form of the *matter power spectrum*. This has allowed its use in real and mock data analyses for galaxy surveys to obtain and forecast constraints on deviations from Λ CDM (Tröster et al. 2021; Spurio Mancini & Bose 2023; Frusciante et al. 2023; Carrion et al. 2024).

Modelling beyond- Λ CDM physics is not the only major challenge. In the nonlinear regime many physical phenomena start to affect matter clustering in a significant way. In particular, the effects of massive neutrinos (Bird et al. 2018, 2012; Blas et al. 2014; Mead et al. 2016a; Lawrence et al. 2017; Tram et al. 2019; Massara et al. 2014; Angulo et al. 2021) and baryons (for example van Daalen et al. 2011; Mummery et al. 2017; Springel et al. 2018; van Daalen et al. 2020; Schneider et al. 2019; Chisari et al. 2019) have been shown to be extremely important. Neglecting any of these effects will lead to biased estimates of cosmology and gravity (Symboloni et al. 2011; Schneider et al. 2020a,b; Martinelli et al. 2021). Fortunately, baryonic effects have been well studied and can be efficiently modelled with the addition of a few degrees of freedom (Aricò et al. 2021; Mead et al. 2020; Giri & Schneider 2021). It also appears they are loosely coupled to modifications to gravity (see Mead et al. 2016b; Arnold & Li 2019, for example). On the other hand, massive neutrinos are known to be highly degenerate with particular modifications to gravity and do couple in non-trivial ways to the gravitational degrees of freedom (see for example Mead et al. 2016b; Wright et al. 2017, 2019). Models for these effects have been tested in tandem with the halo model reaction against various beyond- Λ CDM numerical and hydrodynamical simulations, with very promising agreement ($\sim 3\%$ for $k \leq 1 h/\text{Mpc}$) shown (Bose et al. 2021; Paribelli et al. 2022) at the level of the power spectrum.

1.2 Machine Learning

The aforementioned modelling methods can be implemented in statistical data analyses to derive cosmological parameter constraints, marginalised over a suite of nuisance parameters. Performing statistical analyses such as Markov Chain Monte Carlo (MCMC) on very high dimensional models is not straightforward. Computational expense and complex parameter degeneracies are among the major problems of such analyses, and the efficient sampling of the posterior distribution can be challenging. In addition to the huge number of extra parameters, one deals with a vast model space of cosmological theories. This is where machine learning can help. A trained neural network can be more efficient and preselect models that are worth testing in a MCMC.

A deep neural network (DNN) provides a highly nonlinear map between the input (in this case a cosmological quantity) and the output (in this case a classification of theoretical model). DNNs have shown to be successful in many classification problems, predominantly outside physics (Mehta et al. 2019; Lin et al. 2017; LeCun et al. 2015). Bayesian Neural Networks (BNNs) try to model the uncertainty by replacing each weight in the network by a distribution initialised to a prior (MacKay 1992; Neal 1996; Blundell et al. 2015; Gal & Ghahramani 2016; Charnock et al. 2022; Valentin Jospin et al. 2020). In a previous paper (Mancarella et al. 2020), the authors suggested the employment of BNNs to supplement cosmological MCMC analyses. This works by classifying an input power spectrum using the BNN, and then using that classification to select various degrees of freedom or apply stronger priors on model parameters, both of which can be applied to heighten efficiency of subsequent MCMC analyses.

Using the ReACT code, the authors of Mancarella et al. (2020) built a very large data set of power spectra for various gravitational and cosmological models with 21,000 realisations each. This was then used to train and test a BNN called the **B**ayesian **C**osmological **N**etwork, (BaCoN, ). The authors also implemented a constant systematic error in training which aimed at accounting for theoretical inaccuracies in the beyond- Λ CDM and nonlinear theoretical modelling. This BNN was shown to be remarkably accurate at classifying power spectra into various modified gravity or dark energy models, with a test set accuracy of $\sim 95\%$. Post training, this classification could be done almost instantly given an input spectrum. This suggested that a well calibrated and appropriately trained network could be invaluable in guiding more intensive cosmological analyses.

1.3 Overview

In this work, we extend the training of BaCoN to include massive neutrinos and baryonic effects using the baryonic feedback model described in Mead et al. (2020) and the massive neutrino implementation of ReACT (Bose et al. 2021). We also investigate the most effective way to model the theoretical (systematic) error, going beyond the constant assumption of the previous work. Finally, we also adopt a far more accurate prescription for the power spectrum training data by making use of the state-of-the-art Euclid Emulator (Knabenhans et al. 2021).

This paper is laid out as follows. Section 2 presents our theoretical and numerical setup. Section 3 then describes the data preparation before it can be passed to the BNN, along with a discussion of the BNN's architecture. Section 4 presents our results and discusses the performance of the BNN. Section 5 presents our conclusions and outlines future plans.

2 THEORETICAL SETUP

2.1 Bayesian and Convolutional Neural Networks

A Bayesian neural network combines a neural network with Bayesian statistics. The general idea is that instead of optimising fixed weights for every node the network uses marginal distributions. The two main advantages of BNNs are avoiding overfitting and providing a measure of uncertainty for the predictions. If we pass a sample repeatedly through the network we obtain a distribution instead of a single prediction for the classification result.

BaCoN-II is based on the architecture of convolutional neural networks (CNNs) so it combines Bayesian inference with image analysis in broad terms. A CNN does not fully connect all the nodes of adjacent layers. A convolutional layer convolves the image layer with a smaller set of filters and the recognised features are saved in activation maps.

For BaCoN-II we use a matter power spectrum, $P(k, z)$, at four redshifts as the input image. The network performs its classification based on visual features in the spectrum. The patterns recognised in the convolutional layers are in our case shapes in the power spectrum. This makes the substructure of the graph more important than the overall amplitude. Hence, our choice of network architecture influences what the network is most sensitive to, which will differ from an established cosmological MCMC analyses. This also alters our approach to the noise model, which we will discuss in Section 4.1. In general, it had been expected that CNNs do not keep track of the position of a structure in the input image, but it was shown recently by Islam et al. (2019) that the convolutional layers may implicitly learn absolute position information. This would explain the high accuracy that we obtain when analysing spectral data. Furthermore, Zhou et al. (2016) have developed Class Activation Maps (CAMs) that are able to visualise the areas of the image that were most influential on the classification decision of a CNN. Zhong et al. (2022) have shown that they can be deployed successfully for spectra retrieving position information of class-specific features in the input.

Our network architecture ends with a final fully connected layer to be able to output probabilities for 5 classes. The actual classification is decided by a probability threshold. If one class has a probability above 50% the spectrum counts as being classified. The final output for a test of a trained BaCoN-II network is a *confusion matrix* which shows the percentages of all correctly, wrongly, and not classified spectra. This is ideally a fully diagonal matrix and we can use the off-diagonal entries to interpret degeneracies between classes. The contribution to true positives, false positives, true negatives and false negatives are broken down by the specific classes. We evaluate all our networks using the full confusion matrix for the test data but we will sometimes only state the total test accuracy (true positive rate over all classes) for conciseness.

The architecture and machine learning techniques used here are the same as in our previous work. We point the reader to Mancarella et al. (2020) for the details.

2.2 Halo model reaction

To create our training data we use the approach of Cataneo et al. (2019), which models the nonlinear power spectrum as

$$P_{\text{NL}}(k, z) = \mathcal{R}(k, z) P_{\text{pseudo}}(k, z). \quad (1)$$

Here, \mathcal{R} is the halo model reaction function and quantifies corrections to the pseudo spectrum coming from the nonlinear, non-standard physics in the beyond- Λ CDM universe. We refer the reader to Bose et al. (2021) for the analytic formulae on which this function is based.

It can be efficiently computed using the publicly available ReACT code (Bose et al. 2020, 2022, ). The accuracy of this function was found to be at the 1%-level in Cataneo et al. (2019) for $k \leq 1$ h/Mpc for both modified gravity and dynamical dark energy models.

$P_{\text{pseudo}}(k, z)$ is called the pseudo power spectrum and is defined as a nonlinear spectrum in a Λ CDM universe but whose initial conditions are tuned so that the linear clustering matches the beyond- Λ CDM universe at a given redshift, z . The purpose of using the pseudo power spectrum is to ensure the halo mass functions in both beyond- Λ CDM and pseudo universes are similar, which gives a better transition between linear and nonlinear regimes. This quantity can be modelled using nonlinear formulas such as HMcode (Mead et al. 2015, 2016b, 2020) or halofit (Takahashi et al. 2012), which require the specification of a linear power spectrum, allowing the user to provide the modified linear clustering while keeping the nonlinear clustering based on Λ CDM physics. The drawback is that these fitting formulae introduce a significant inaccuracy in the calculation. These inaccuracies have been qualified at 5% in both cases for $k \leq 1$ h/Mpc, but with HMcode typically achieving a higher $\sim 2.5\%$ accuracy for most cosmologies (Mead et al. 2020; Takahashi et al. 2012). These inaccuracies dominate the error budget of Equation 1.

In Mancarella et al. (2020), the authors used the halofit formula to generate the training set, and account for theoretical uncertainties using a constant systematic. This was highly underestimated as we highlight in Section 4.1. In addition to improving the error prescription, we also improve upon the ‘old’ training data by using two, improved prescriptions for our predictions.

The first employs the improved HMcode formula of Mead et al. (2020)

$$P_{\text{NL}}^{\text{HMcode2020}}(k, z) = \mathcal{R}(k, z) P_{\text{pseudo}}^{\text{HMcode2020}}(k, z). \quad (2)$$

We expect this prediction to be $\sim 6\%$ accurate for $k \leq 1$ h/Mpc as we consider a wide range of cosmologies. In particular, the pseudo cosmologies may have a fairly large amplitude of linear clustering due to enhancements from modified gravity forces. This will affect the accuracy of the pseudo power spectrum as noted in Atayde et al. (2024); Tsedrik et al. (2024). This accuracy increases to $\geq 9\%$ for $k \leq 3$ h/Mpc as estimated from Cataneo et al. (2019), which did not include massive neutrinos.

The second also employs HMcode, but as a ratio of modified-to- Λ CDM predictions, i.e., a boost. This effectively factors out some of the inaccuracy inherent in the HMcode prediction. To get P_{NL} we then multiply the HMcode-based boost with a highly accurate prediction for $P_{\text{NL}}^{\Lambda\text{CDM}}$. This is available via the sophisticated Λ CDM power spectrum emulator, EuclidEmulator2 (Knabenhans et al. 2021) (EE2), which efficiently emulates N -body predictions for Λ CDM cosmologies. This ‘optimal’ accuracy version for the spectra predictions is then given as

$$P_{\text{NL}}^{\text{EE2}}(k, z) = B^{\text{HMcode2020}}(k, z) \times P_{\Lambda\text{CDM}}^{\text{EE2}}, \quad (3)$$

where

$$B^{\text{HMcode2020}}(k, z) \equiv \frac{\mathcal{R}(k, z) P_{\text{pseudo}}^{\text{HMcode2020}}(k, z)}{P_{\Lambda\text{CDM}}^{\text{HMcode2020}}(k, z)}. \quad (4)$$

EE2 is $\sim 1\%$ accurate for $k \leq 10$ h/Mpc for Λ CDM cosmologies. The HMcode boost was found to have an accuracy of $\sim 2\%$ for a range of gravitational and dark energy theories including massive neutrinos, for $k \leq 1$ h/Mpc (Bose et al. 2021). This gives us an estimated accuracy of 3 – 4% for $k \leq 1$ h/Mpc. This degrades to $\sim 6\%$ for $k \leq 3$ h/Mpc (Bose et al. 2021). From these references we estimate an accuracy of 5% for $k \leq 2.5$ h/Mpc, which will be used in Section 4.

In this work we consider both Equation 2 and Equation 3 to train our network, and importantly use both of these predictions to calibrate the theoretical error assumed in the network’s predictions. The effects of massive neutrinos and beyond- Λ CDM physics are primarily included in \mathcal{R} , but also in the linear spectrum that goes into P_{pseudo} . We also look to include the effects of baryonic physics, which is known to greatly affect the matter power spectrum at non-linear scales (Schneider et al. 2019, 2020b,a). This can now easily be included via $P_{\text{pseudo}}^{\text{HMcode2020}}$ through the single-parameter baryonic feedback modelling available within HMcode (Mead et al. 2020). This is a less comprehensive modelling of feedback processes than the more sophisticated emulators such as those of Aricò et al. (2021); Giri & Schneider (2021), but will serve as a first test of our network’s capacity to distinguish between baryonic physics, massive neutrinos and non-standard physics. We leave more sophisticated feedback modelling to a future work.

2.3 Data Sets

We will consider 5 classes of cosmological and gravitational models, following Mancarella et al. (2020):

(i) Λ CDM, which assumes general relativity as the underlying gravitational model.

(ii) The Hu-Sawicki $f(R)$ gravity model (Hu & Sawicki 2007), parametrised by the value of the additional scalar field today, f_{R0} . This model exhibits the Chameleon screening mechanism (Khoury & Weltman 2004). We assume a Λ CDM background for this model.

(iii) The normal branch of the Dvali-Gabadadze-Porrati (DGP) brane-world model (Dvali et al. 2000), parametrised by $\Omega_{rc} = 1/(4r_c^2 H_0^2)$, where H_0 is the Hubble constant and r_c is a scale governing where gravitational interactions begin to dilute into the 5-dimensional bulk. This model exhibits the Vainshtein screening mechanism (Vainshtein 1972). We assume a Λ CDM background for this model.

(iv) An evolving dark energy model as parameterised in Chevalier & Polarski (2001); Linder (2003) (w CDM), with the parameter pair $\{w_0, w_a\}$ giving the value of the dark energy equation of state today and its time evolution respectively, where $w(a) = w_0 + (1-w_0)w_a$, a being the scale factor of the FLRW metric. Here the background is distinct from Λ CDM.

(v) A random class as considered in Mancarella et al. (2020), but with slightly different settings as described in Sec. A. This class aims to capture any unknown/unconsidered models of gravity or dark energy whose phenomenology is largely distinct from the other classes. The new features are correlated in their redshifts and scales instead of being completely random. Hence these spectra can be interpreted as the ‘other’ class that represents feasible other models with new physics.

For each of these scenarios we consider different sets of baseline Λ CDM cosmological parameters, $\{\Omega_m, \Omega_b, H_0, n_s, A_s\}$ - the total matter fraction, the total baryonic matter fraction, the Hubble constant, the spectral index and the primordial amplitude of perturbations, respectively. In addition to these, we also include the effects of massive neutrinos, parametrised by the sum of the neutrino masses $\sum m_\nu$, as well as baryonic feedback effects, parametrised by the T_{AGN} parameter of HMcode.

We sample these parameters to generate large sets of power spectra for each scenario. The parameters are sampled from Gaussian distributions with the following means and standard deviations:

$\{\Omega_m, \Omega_b, H_0, n_s, A_s\}$ are sampled using the Planck 2018

(Aghanim et al. 2020b) best fits as a mean and we take the standard deviation forecasted for the combination of weak lensing and spectroscopic clustering probes of the Euclid mission (Blanchard et al. 2020a). When using Equation 3 we also impose the hard EE2 priors, which particularly restrict $\Omega_b \in [0.04, 0.06]$.

$\{\Omega_{rc}, f_{R0}\}$ are sampled with their Λ CDM-limits as a mean ($\Omega_{rc} = f_{R0} = 0$, though the mean itself is not part of the data set) and a standard deviation taken to be the 3σ cosmic shear constraint forecasted for an LSST-like survey in Bose et al. (2020) using only linear scales.

$\{w_0, w_a\}$ are sampled using their Λ CDM-limits ($\{w_0, w_a\} = \{-1, 0\}$) and the standard deviation is taken to be the value forecasted for the combination of weak lensing and spectroscopic clustering probes of the Euclid mission (Blanchard et al. 2020a). We also impose the following hard limits to ensure stability of the ReACT code, $w_0 \in [-1.3, -0.7]$ and $w_a \in [-1.5, 0.3]$.

The $\sum m_\nu$ parameter is taken to have the same standard deviation and mean as the fiducial value assumed in Blanchard et al. (2020a), a lower bound estimate based on observations from neutrino oscillation experiments (Esteban et al. 2020). In parameter files we quote the massive neutrino energy density fraction today, Ω_ν , with $\sum m_\nu = \Omega_\nu h^2 93.14$ eV.

The baryonic parameter $\log_{10}[T_{\text{AGN}}]$ is taken to have the default mean value of HMcode, 7.8, and a standard deviation covering the fits to the BAHAMAS simulations (McCarthy et al. 2017) given in Mead et al. (2020).

These choices aim to give an estimate of what the BNN can achieve given the data from forthcoming galaxy surveys such as Euclid and VRO/LSST, while remaining consistent with the Planck CMB observations. The parameter ranges are summarised in Table 1. We demonstrate the effects of dynamical dark energy, modified gravity, massive neutrinos and baryonic feedback on the matter power spectrum in Section B. Figure B1 shows the characteristic changes of P_{NL} when the model parameter is varied, keeping the baseline cosmological parameters constant.

We generate power spectra for all these scenarios using the following codes (see Equation 2 and Equation 3):

- (i) \mathcal{R} is computed using ReACT .
- (ii) $P_{\text{pseudo}}^{\text{HMcode2020}}$, $B^{\text{HMcode2020}}$ and the baryonic boost are computed using HMcode .
- (iii) $P_{\text{ACDM}}^{\text{EE2}}$ is computed using EE2 .
- (iv) The modified linear spectra with massive neutrinos are computed using MGCAMB  for the Λ CDM, $f(R)$ and w CDM scenarios.
- (v) The DGP linear spectra were generated using a private, modified version of CLASS (Lesgourgues 2011; Blas et al. 2011) which was also employed in Frusciante et al. (2023).

On the data repository [here](#) we include the pipelines used to generate spectra for all scenarios and using both Equation 2 and Equation 3.

Each power spectrum data file is generated using a parameter set sampled from the ranges detailed in Table 1. These data files, used for both training and testing of the network, have a shape of 5 columns \times 500 rows. The first column is the values of the Fourier mode sampled in h/Mpc , where we sample logarithmically in the range $[0.01, 10] h/\text{Mpc}$. The 2nd to 5th columns are the values of the power spectrum at those Fourier modes, with each column corresponding to the following redshifts $z \in \{1.5, 0.785, 0.478, 0.1\}$. These redshifts are chosen to roughly sample the range of tomographic bins Euclid’s weak lensing survey will be making measurements at (Laureijs et al. 2011; Blanchard et al. 2020b), with an omission of the highest bins which can go beyond $z = 2$. We do not expect strong beyond- Λ CDM

effects at high redshift, but aim to consider this in a more comprehensive future iteration of the network where we train directly on the observables and not the matter power spectrum.

The complete list of data sets available [here](#) is summarised in [Table 2](#).

3 TRAINING THE NETWORK

The whole process from data generation to training and testing the classification network is displayed as a scheme in [Figure 1](#). We will describe all the involved stages in this section. Some steps are marked with blue boxes in the graphic and are discussed in the following subsections. We will go through the specific influences of these marked parts in [Section 4](#).

3.1 Data Generation

The theoretical background of the data generation has been described in [Section 2.2](#). Here, we will only address the practical choices. We start by drawing cosmological parameters from the priors for Λ CDM. This set of parameters is then fed into a code to produce a nonlinear Λ CDM matter power spectrum (either EE2, or HMcode, or `halofit`). Then we choose the cosmological class that we want to generate matter power spectra for. This can be $f(R)$, DGP, w CDM or Λ CDM and draw from the class-specific parameter distribution. If we want to include effects of massive neutrinos and baryonic feedback, we include their respective parameters as well. All parameters are then passed on to ReACT and HMcode to calculate the boost. Finally, this is combined with the Λ CDM spectrum to get a nonlinear matter power spectrum for the selected class.

3.2 Noise Model

We normalise the power spectra data with a generic matter power spectrum to reduce the dynamic range of the data presented to the BaCoN-II network. Throughout this work, we use the same Λ CDM normalisation spectrum. We have tested the influence of different normalisation spectra including a linear matter power spectrum without Baryonic Acoustic Oscillations (BAOs). There is no noticeable effect as long as the same normalisation is used for the training and the testing phases. We set the default normalisation spectrum as an EE2 Λ CDM spectrum with the Planck cosmology ([Aghanim et al. 2020b](#)) without baryonic feedback or massive neutrinos.

For every normalised spectrum we produce 10 realisations sampled from our *noise model*. This model has two components:

The first component represents noise coming from a Stage IV-like survey’s cosmic variance. This component is given by

$$\sigma_p(k) = \sqrt{\frac{4\pi^2}{k^2 \Delta k V(z)}} \times P(k), \quad (5)$$

where $V(z)$ is the volume probed at a given redshift and Δk is the bin-width. The Stage IV-like volumes we adopt are: $V(1.5) = 10.43 \text{ Gpc}^3/h^3$, $V(0.785) = 6.27 \text{ Gpc}^3/h^3$, $V(0.478) = 3.34 \text{ Gpc}^3/h^3$ and $V(0.1) = 0.283 \text{ Gpc}^3/h^3$ ([Laureijs et al. 2011](#); [Blanchard et al. 2020b](#)). We do not consider shot noise as we are using dark matter spectra, whose associated particle density is very large.

The second component is used to model the theoretical uncertainty in our power spectra predictions. As stated in [Section 2.2](#), all terms used in the power spectra model have associated inaccuracies that contribute to the overall theoretical error of our nonlinear matter power spectra predictions. This becomes very apparent when we look at the difference of power spectra predictions based on EE2 and HMcode as displayed in [Figure 2](#). Both codes produce characteristic fingerprints in the spectrum and deviate from each other by up to 4%. To avoid a fitting of the neural network to these prescription-specific errors, we generate curves with similar features to model such theoretical errors in the training process. The development of our theoretical error models will be discussed in detail in [Section 4.1](#). These theory error curves are rescaled with a factor which we treat as a parameter to vary, and which accounts for potential errors of different amplitudes.

Note that while we add cosmic variance to the test data before passing it through the network, we do not add the theoretical error component. This is because the test data should be treated the same way as observational data that will be passed through the network for classification.

3.3 Neural Network

We train the BNN with the noisy training data. The shape of the data can be adapted at this stage, *e.g.* with scale cuts. We employ a training data set of 20,000 spectra per class (of which 15% are used as a validation set) to train our most accurate models. The architecture of the BNN, hyperparameters, loss function etc. remain unchanged from the initial BaCoN and are described in detail in [Mancarella et al. \(2020\)](#). We train the network for 50 epochs or until the training accuracy has become stationary. This is the most time consuming part of the machine learning process. The list of data sets used for training and testing is displayed in [Table 2](#) and has been made publicly available [here](#).

Once we have trained the network, we test it with the noisy test data. As in [Mancarella et al. \(2020\)](#), every example requires a classification probability of 50% or above to be considered as classified. Otherwise we count it as not classified (N.C.). After passing all 1000 test data spectra through the network with 10 noise realisations each, we obtain the confusion matrix for this test set. We will present the test results for many different models and tests in the next section.

We conclude this overview with a list of all changes in our methodology in comparison to [Mancarella et al. \(2020\)](#):

- (i) Improved physics in the data generation (massive neutrinos and baryonic effects).
- (ii) Codes with higher accuracy for the Λ CDM spectra computation (EE2 and HMcode instead of `halofit`).
- (iii) Improved random spectra (see [Section A](#)).
- (iv) Different model for the theoretical error and no shot noise term is included in training.
- (v) We only add the theoretical error to the training data and not to the test data.

We will present the theoretical error model, results for our baseline model and the influence of the blue marked components in [Figure 1](#) in the next section.

4 RESULTS

In this section, we will investigate how the classification result is affected by the various influences outlined in [Section 3](#) and [Figure 1](#).

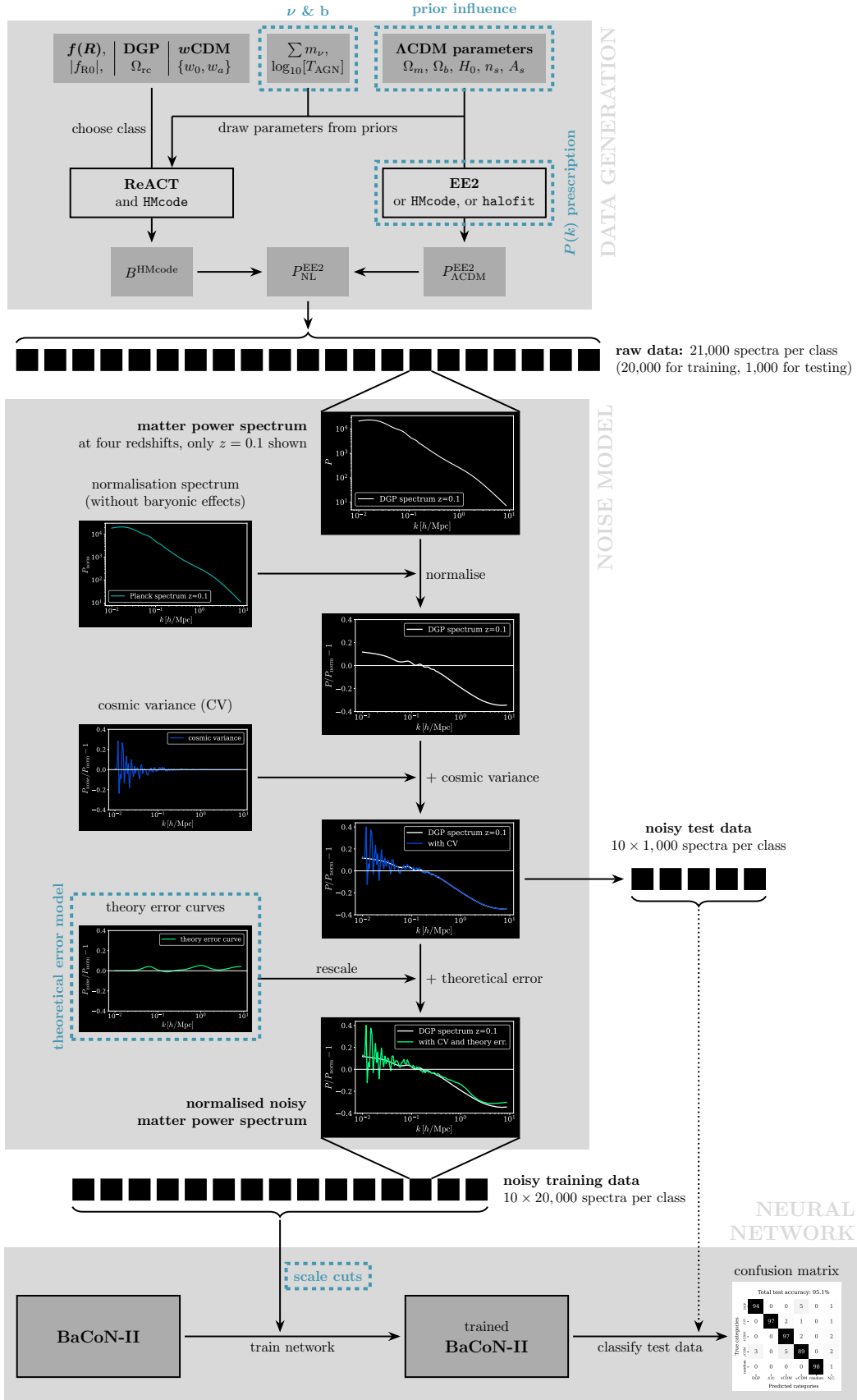


Figure 1. Flowchart of the full pipeline from data generation to the final classification result. The noise model is demonstrated on a DGP spectrum. See Section 3 for a detailed explanation.

Table 1. Parameter ranges for BaCoN-II data. These are sampled assuming a Gaussian distribution with means and standard deviations given below. The fiducial (mean) cosmology (without baryons but with massive neutrinos) gives a $\sigma_8(z=0) = 0.812$, which is the Planck 2018 best fit. We normalise with a Λ CDM spectrum with $\sum m_\nu = 0$, where we use $A_s = 2.025 \times 10^{-9}$ to get $\sigma_8 = 0.812$. Hard limits are placed on w_0 and w_a as described in the main text to ensure stability of ReACT. When using EE2, Ω_b is also restricted to the emulator range of [0.04, 0.06].

Parameter	Mean	Std. Dev.	Reference & Notes
Ω_m	0.3158	0.009	Table. 1 of Aghanim et al. (2020b) (Planck, best fit) & Table. 9 of Blanchard et al. (2020b) (GC _s + WL, pessimistic)
Ω_b	0.0494	0.016	We use $\sigma_{\text{Planck}}/2$ as large Ω_b leads to computational issues in ReACT.
H_0 [km/s/Mpc]	67.32	0.41	
n_s	0.966	0.007	
A_s	2.199×10^{-9}	2.199×10^{-11}	Mean cosmology corresponds to $\sigma_8 = 0.812$. We convert % error on σ_8 to A_s .
$ f_{R0} $	10^{-10}	$10^{-5.5}$	Λ CDM-limit mean and 3σ , $\ell_{\text{max}} = 500$ from Table. 2 of Bose et al. (2020)
Ω_{rc}	10^{-10}	0.173	Λ CDM-limit mean and 3σ , $\ell_{\text{max}} = 500$ taken from chains of Bose et al. (2020)
$\{w_0, w_a\}$	$\{-1, 0\}$	$\{0.097, 0.32\}$	Λ CDM-limit mean and & Table. 11 of Blanchard et al. (2020b) (GC _s + WL, pessimistic)
$\sum m_\nu$ [eV]	0.06	0.06	Fiducial of Blanchard et al. (2020b) and take same for Std. Dev.
$\log_{10}[T_{\text{AGN}}]$	7.8	0.2	Range of BAHAMAS simulation from Table. 4 of Mead et al. (2020) .

Table 2. Data sets available ([here](#)) and used in this work.

P(k) prescription	Classes	Set size	Notes
HMcode-based	All	20,000	Main training set
HMcode-based	All	1,000	Main test set
EE2-based	All	20,000	Main training set
EE2-based	All	1,000	Main test set
EE2-based	Λ CDM	20,000	No baryons or massive neutrinos
EE2-based	All	1,000	No baryons or massive neutrinos
halofit-based	All	19,900	No baryons or massive neutrinos, used in Mancarella et al. (2020)

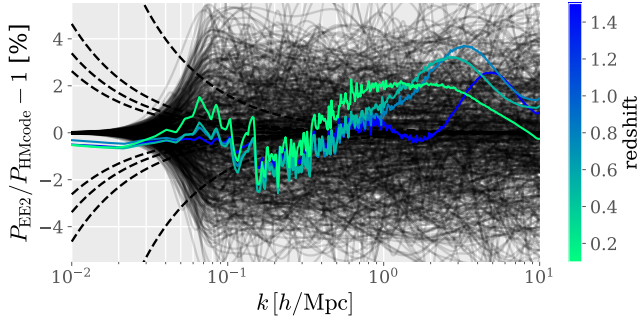


Figure 2. Effects of the power spectrum prescription and the theoretical error model: Ratio of EE2 and HMcode Λ CDM spectra at different redshifts for the same cosmological parameters shown as coloured lines. The dashed lines show the 1σ level of cosmic variance (see [Equation 5](#)) at the 4 redshifts considered in this work and the black lines are 600 possible theory error curves scaled to 5%. Note the noise in the EE2-HMcode ratio is noise inherent in the EE2 spectra emulation.

We evaluate the network performance using the full confusion matrix, but for clarity we will often only state the total classification accuracy (true positive rate) in the figures. A note on reproducibility of the numbers in this section: The scatter of classification accuracies is very low. When retraining and retesting the network with data produced using the same power spectrum prescription, the total accuracy varies by less than 1%. The variability of test results can go up to 4% when testing on data produced using a different spectrum prescription than used in training. We expect this variability to decrease through the refinement of our theoretical error model, which should suppress the influence of the specific power spectrum prescription.

4.1 Theoretical Error Model

Before we move to the main classification results for our baseline model, we will explain the shape of the curves that we use to model the theoretical error component in our noise model. This has gone through several stages of development and we show all of them as they provide insights into the nature of this error. [Figure 3](#) shows the different shapes of the models we have considered, which are discussed shortly. Curves generated using these models are added to the noisy spectra before training as highlighted in [Figure 1](#). We once again emphasise that they will only be added to the training data and not to the test data, as the latter is meant to represent actual observations.

To test the effectiveness of our theoretical error model, we trained networks on a reduced EE2 training set (1,000 spectra per class) and added the curves for the theoretical error scaled to different percentages. These networks were then tested with EE2 and HMcode test data. As shown in [Figure 2](#), there is a considerable systematic difference between EE2 and HMcode matter power spectra - for $k_{\text{max}} = 2.5 h/\text{Mpc}$ this is estimated to be roughly 5%. This difference is representative of the potential error when comparing our spectra prescription to the real Universe. If we model the theoretical error well enough, the accuracies for the two test data sets should converge when the amplitude of the error in training is increased, without reducing the overall accuracy significantly.

In [Mancarella et al. \(2020\)](#) the authors employed a Gaussian noise similar to our treatment of cosmic variance, with a constant component associated with the theoretical uncertainty. The top panel in [Figure 3](#) shows that after normalisation this leads to an underestimate of the error on BAO scales and an extremely large error at very small scales. We first attempted to correct this by scaling the constant contribution by the normalisation matter power spectrum. This gives us a Gaussian error of the same amplitude at all scales, which is shown in the second panel.

In [Figure 4](#) we show the test accuracies for this Gaussian error

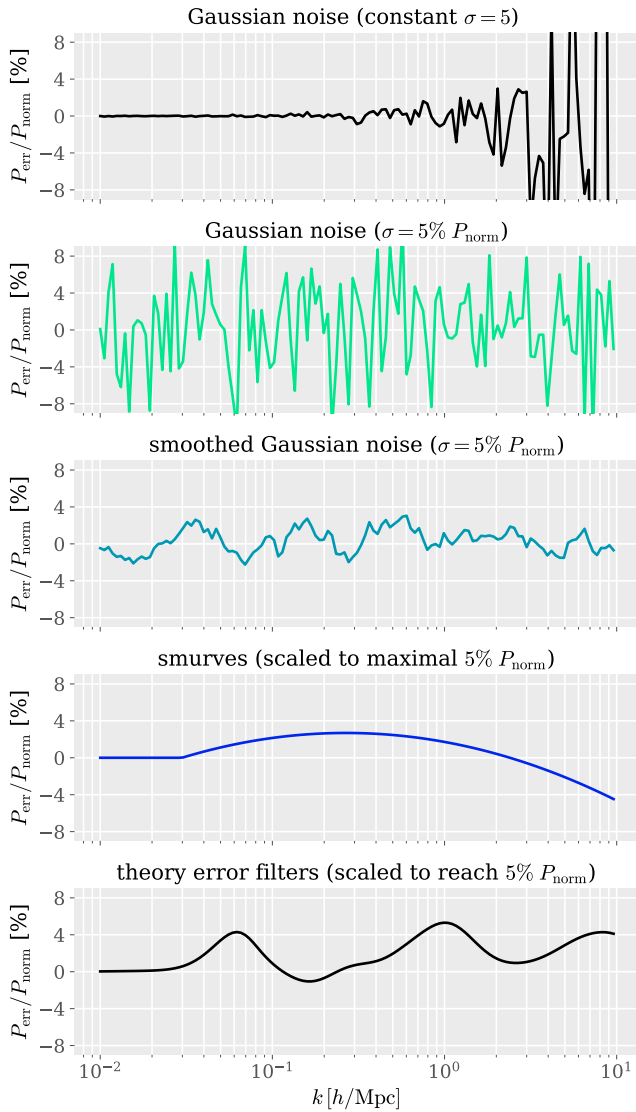


Figure 3. Theoretical error models: Development stages of curves added to the training data that account for the theoretical uncertainty in our training data power spectra predictions. All models are scaled to an equivalent of 5% of a Λ CDM Planck normalisation spectrum and are plotted after normalisation.

model as a function of the overall error amplitude (in this case the standard deviation of the Gaussian). We note the accuracy falls off drastically when we increase the standard deviation. We have found that this decrease does not happen when we add the same noise to the test spectra. This suggests the dropping accuracies are resulting from the missing noise in the test data compared to the training data. The network has over-trained on the structure of the Gaussian noise and is not able to generalise to noise-free spectra.

To try to mitigate this, we then smoothed the Gaussian noise as shown in the middle panel of Figure 3. However, the testing results plotted in Figure 4 are unaffected by the smoothing. The shapes introduced by this kind of noise still seem to be too distracting for the network. Different smoothing scales had no effect on this trend either.

To overcome this problem, we opted for a completely smooth error curve displayed in the second lowest panel of Figure 3. These curves

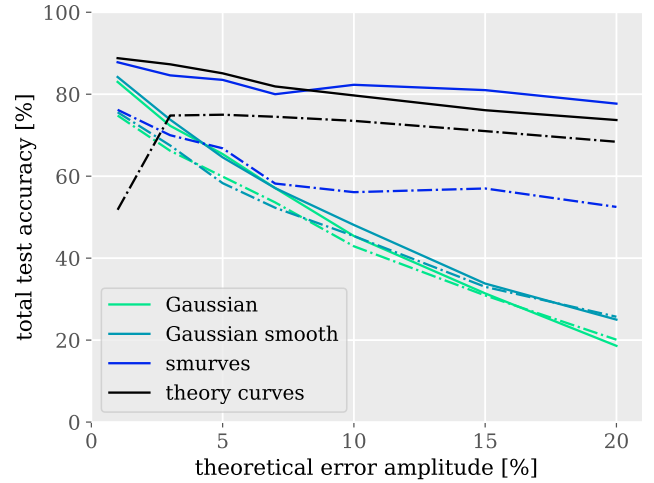


Figure 4. Model accuracy under various noise models for the theoretical error: Dependence of total test accuracy on the size of the theoretical error for different theory error models. Representatives of the curves corresponding to each model are shown in Figure 3 with the same colour coding. All models have been trained with a subset of the main EE2 training data (1000 training spectra per class). The testing was conducted without adding a theoretical error, using EE2 (solid line) or HMcode test data (dashed-dotted line).

have been produced with a modification of the smurves package that was developed by Moews et al. (2019) (©). We then scale these curves by an overall amplitude factor which we vary, as in the Gaussian error case. These parabola-like shapes have no substructure that the network could become over-fit to. The test accuracy for EE2 data remains high even for large error amplitudes. However, the HMcode tests plotted in Figure 4 have a large decrease in accuracy and are nowhere near convergence with the EE2 accuracies. We deduce that the smurve curves do not distract the network but on the other hand do not add enough features to capture the systematic error between EE2 and HMcode spectra.

Finally, we test a combination of both approaches and produce smooth curves with features to represent real theoretical uncertainties in the prescription of the matter power spectrum. These are generated using a slightly modified algorithm as used to generate the random class (see Section A). These theory error curves are shown in the bottom panel of Figure 3. The EE2 test results in Figure 4 are of similar high accuracy to the smurve model. There is a small decrease towards very high amplitudes as we would expect. The HMcode-results now, for the first time show converging accuracy to the EE2 test set, when adding more systematic noise. This indicates that the theory error curves are a step in the right direction, towards mimicking generalised theoretical uncertainties (as represented in this case by the difference between EE2 and HMcode spectra).

In fact, we have plotted a number of ‘theory error curves’ in the background of the EE2-HMcode ratio in Figure 2 for comparison. While the long-wavelength features in the EE2-HMcode ratio itself are well represented, we can see that there are some short-wavelength, fine structure in the error that we have not captured. This is likely responsible for the remaining accuracy discrepancy of $\sim 5\%$ between the EE2 and HMcode test results, present even when we add theory error curves that are scaled up to 20% of the normalisation spectrum. However, the overall desired effect of the theoretical error component has been achieved.

Total test accuracy: 95.1%

True categories	DGP	94	0	0	5	0	1
	$f(R)$	0	97	2	1	0	1
	Λ CDM	0	0	97	2	0	2
	w CDM	3	0	5	89	0	2
	random	0	0	0	0	98	1
		DGP	$f(R)$	Λ CDM	w CDM	random	N.C.
		Predicted categories					

Figure 5. Confusion matrix of the baseline EE2-based model (see Equation 3) trained with 5% theoretical error component and tested with the main EE2 test data. We use data up to $k_{\max} = 2.5 h/\text{Mpc}$ for training. The class accuracies are shown in percent. (N.C. stands for ‘Not Classified’).

All the tests that we will discuss in the following sections have been made with networks trained with theory error curves as the theoretical error component to our noise model, added in to the training spectra.

4.2 Cosmological Model Classes

The main test result of our EE2 baseline model is shown in Figure 5. The model has been trained with a 5% theoretical error based on the theory error curves and we have used a scale cut at $k_{\max} = 2.5 h/\text{Mpc}$. The total test accuracy is 95.1% and the confusion matrix is mostly diagonal. Overall, the trained BaCoN-II network can successfully classify a very high proportion of matter power spectra from all classes. As the strength of modifications in the training data are drawn from a Gaussian around Λ CDM (see Table 1 for the parameter distributions), this result shows a high capability of correctly identifying new physics beyond Λ CDM even for small deviations.

To understand the few misclassifications, we can study the characteristic effects of each beyond-standard-model class on the matter power spectrum that is displayed in Figure B1. Dynamical dark energy can produce a similar amplitude shift to DGP at large scales so the two models are slightly degenerate. Additionally, the w_0 parameter allows for values very close to a cosmological constant so that 5% of w CDM spectra get misclassified as Λ CDM. Both effects reduce the true positive rate of the w CDM class. Hence, w CDM ends up with the lowest class accuracy. Nevertheless, the overall classification result is remarkable. Given that all cosmological parameters are varied at the same time as the class specific parameters, there are fewer degeneracies than one might expect. This shows that the visual analysis of a matter power spectrum that is performed by the convolutional neural network contains enough class specific information that allows for a robust distinction of the cosmological models.

We use this main test of the baseline model as a reference for the various effects that we will investigate next. An overview of all the confusion matrices that will be discussed in the coming sections is given in Figure 8. Our main test result (Figure 5) is shown in the upper

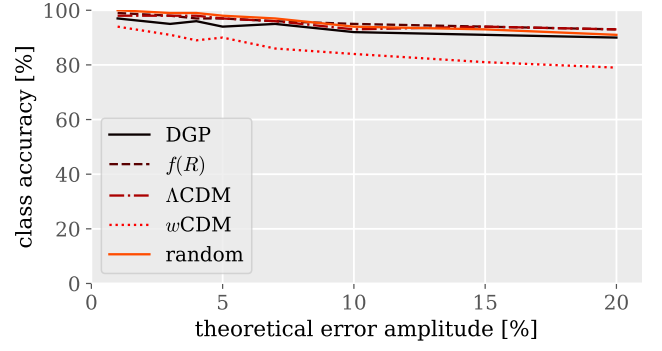


Figure 6. Influence of theoretical error amplitude on class accuracies: EE2 test accuracies for correct class classifications of an EE2 model with added theory curves in training (20,000 training spectra per class) with a scale cut at $k_{\max} = 2.5 h/\text{Mpc}$. The EE2 test and training data have the same cosmological parameter distributions.

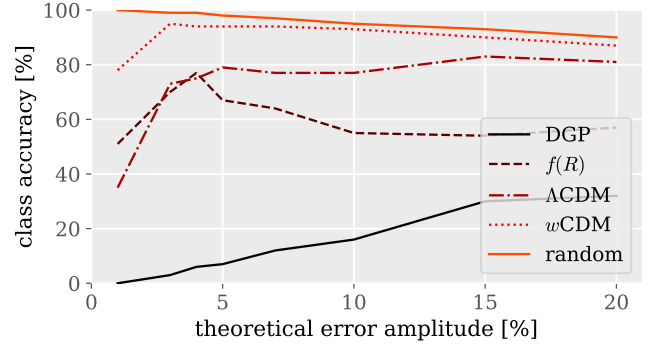


Figure 7. Influence of theoretical error amplitude on class accuracies: HMcode test accuracies for correct class classifications of an EE2 model with added theory curves in training (20,000 training spectra per class) with a scale cut at $k_{\max} = 2.5 h/\text{Mpc}$. The HMcode test and EE2 training data have the same cosmological parameter distributions.

left corner for comparison. All the displayed models are trained with theory error curves scaled to 5%.

Before we move on we have a final look at the class-specific accuracies in the baseline EE2 model. We have plotted the dependency of the class accuracies on the amplitude of the theoretical error for the EE2 test data in Figure 6 and for HMcode test data in Figure 7. When tested with EE2, the accuracies barely drop with a larger theoretical error amplitude. Only w CDM has an accuracy below 90% for the reasons discussed above. When tested with HMcode, we see a stronger class dependency. DGP has a very low accuracy that rises significantly with an increase of the error amplitude, while the $f(R)$ accuracy is reduced at high amplitudes. The latter class has mostly an effect on the power spectrum on smaller scales so it gets proportionally more affected by the amplitude level. The strong differences between the classes in the HMcode case show that the theoretical error influences the fingerprints of the different cosmological models on the matter power spectrum to a very different extent.

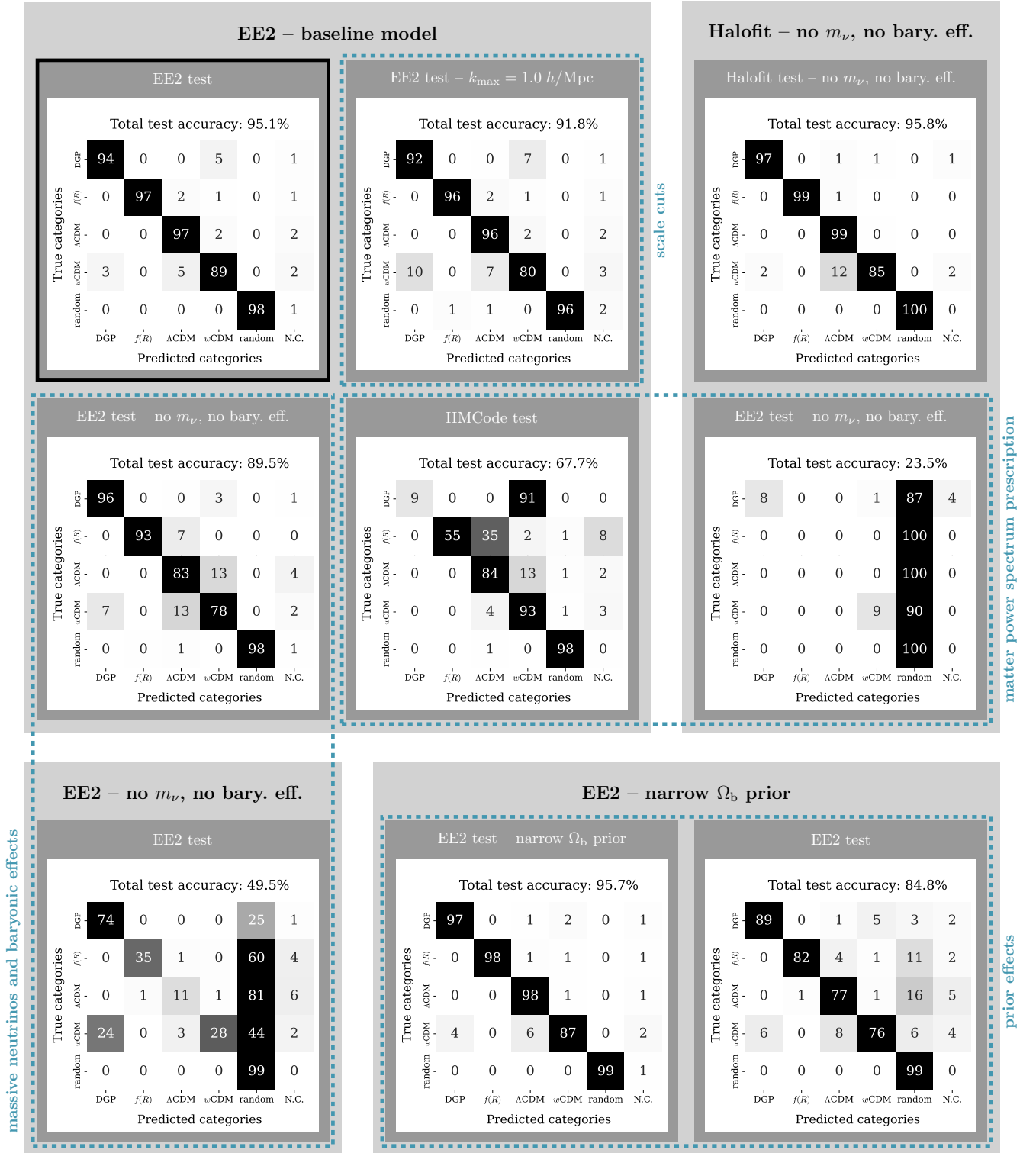


Figure 8. Overview of confusion matrices from testing various models with different training and testing data. All the shown models include theory curves scaled to 5% as a theoretical error component in the noise model added during training, and the new random class based on EE2 Λ CDM spectra with baryons and neutrinos. Light gray boxes indicate the training data, dark gray boxes the test data. The blue dashed frames show which trends are investigated with these models/tests. The main baseline test result is shown in the upper left corner. Class accuracies are shown in percent. (N.C. is ‘Not Classified’). The scale cut is at $k_{\max} = 2.5 h/\text{Mpc}$ if not specified otherwise.

4.3 Massive Neutrinos and Baryonic Feedback

One of the main motivations for this updated version of BaCoN-II was the inclusion of effects from massive neutrinos and baryonic feedback in our description of the matter power spectrum. The total test accuracy of $\sim 95\%$ for the updated spectra shows that the addition of these effects generates no significant loss in accuracy.

If we test a network trained with massive neutrinos and baryonic feedback but without these effects in the test data, there is only a slight 5% decrease of the accuracy as can be seen in the confusion matrix in Figure 8. On the other hand, for a network trained on spectra without the effects of massive neutrinos and baryonic feedback but tested on data with these effects we see a drop of the test accuracy to only 50%. Most classes get predominantly classified as random. This can be explained by the construction of the random spectra based on Λ CDM spectra that include the neutrino mass and baryon modelling parameters. Hence, we see that the characteristic mark of neutrinos and baryons in the matter power spectrum has a stronger impact on the classification than any class specific features. As a consequence, the inclusion of all known physical effects in the data modelling is important to be able to distinguish between beyond- Λ CDM models. However, the effect of massive neutrinos and baryons can be interpreted as an unknown ‘new physics’ from the perspective of a network that is trained without them. Hence, this result shows the capability of the random class to flag the presence of new physics that is missing in the other selected classes.

Also, we have to make sure that the random class is constructed from accurate spectra including all the relevant effects. The only exception in this specific case shown in the test result in Figure 8 is DGP. It still has a high true positive rate as it is mostly affecting the large scales while massive neutrinos, and especially baryonic feedback, impact the smaller scales. This can be seen in Figure B1.

4.4 Power Spectrum Prescription

We will make use of the known systematic difference between the EE2 and HMcode matter power spectrum, shown in Figure 2, to test the effectiveness of our theoretical error model. This difference is found to be largely independent of the cosmological parameters. We add this fixed EE2-HMcode ratio to EE2 test data sets, scaling the ratio to 1% and 3% (the actual ratio shows roughly a $\sim 4\%$ difference). The expectation is that testing the EE2 baseline model on these sets should exhibit an overall accuracy trend that tends towards the HMcode test set.

In Figure 9 we show the test results of the EE2 baseline model for EE2 test sets with these specific systematic errors added in. As expected, smaller systematic differences between the training and test spectra lead to a higher accuracy. Increasing the amplitude of the theory error curves in training reduces the accuracy difference to EE2 test data but still does not fully converge in the case of the 3% EE2-HMcode systematic added to the test set. This indicates that our theory error curves have the desired effect but they are not able to account for the full systematic difference between these two power spectra prescriptions, and so are likely not general enough to be used on real Stage-IV data without incurring some bias in the classification. This lack of convergence can most likely be attributed to the ‘short-wavelength’ features that are visible in the systematic EE2-HMcode difference seen in the coloured curves of Figure 2.

On the other hand, if we are training and testing a network with the same code, we get consistently good classification results. Figure 8 shows confusion matrices for a test of a *halofit* network with *halofit* and EE2 test data. The *halofit* test gives a total classifi-

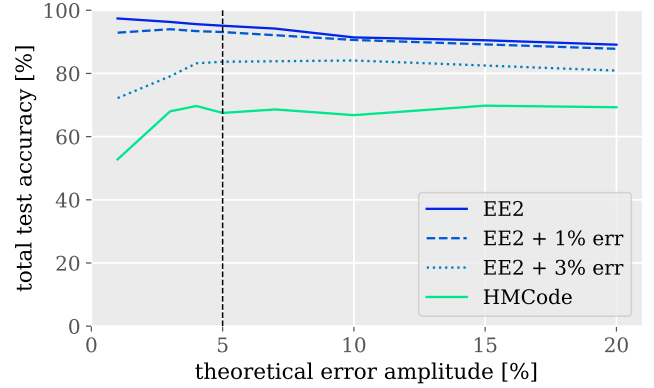


Figure 9. Influence of power spectrum prescription and theoretical error: Total test accuracy of the EE2 baseline model depending on the scaling of the theory error curves added to the main EE2 training data (20,000 training spectra per class). We use EE2 and HMcode test sets as well as the EE2 test set with an added and scaled fixed EE2-HMcode difference (as in Figure 2). 5% is marked as the theoretical error amplitude where the ideal theoretical error model would show convergence of the various test set accuracies.

cation accuracy of $\sim 96\%$ which is nearly identical to the results in Mancarella et al. (2020). Hence, our changes to the pipeline have not reduced the classification power of the BNN. In contrast, a *halofit* network classifies all of the EE2 test spectra as random. This is not surprising as the random spectra are based on EE2 Λ CDM spectra but it shows that the effect of the power spectrum prescription is dominant over the characteristics of the different cosmological classes.

Motivated by these findings, we put the network to another test: comparing data produced with the ReACT pipeline compared to spectra computed directly with an emulator. This is a robustness test to see if the more accurate emulator power spectra can be correctly classified by our trained network. Specifically, we swap the w CDM spectra in our test set without baryons and massive neutrinos with 1000 w CDM spectra produced by EE2 (this should not be confused with our EE2 labelled test data set before, as this is based on EE2 Λ CDM spectra but did still require corrections from ReACT for the different cosmological models). The normalised difference between an EE2 w CDM spectrum and an ReACT-EE2 w CDM spectrum for the same cosmological parameter values is shown in Figure 10. Even for the selected example with a strong deviation from Λ CDM, the difference between the two matter power spectrum prescriptions barely reaches 1%. We will now check if our test results change when we swap the w CDM class in our test data for the more accurate emulated spectra. Figure 11 shows the class test accuracies for the ReACT-EE2 and EE2 w CDM spectra. The network is coping well. Already for the model trained with a 1% theory error the emulated test data has only a 2% drop in accuracy. This vanished when adding larger theory errors during the training of the network. Even though the absolute difference between these w CDM test sets is small as seen in Figure 10, it is reassuring that the network can generalise to more accurate prescriptions and the small theory error gets fully compensated by adding theory error curves during training.

4.5 Scale cuts

We train two EE2 models with scale cuts at $k_{\max} = 2.5 h/\text{Mpc}$ and $k_{\max} = 1.0 h/\text{Mpc}$. Figure 8 displays the confusion matrix for both

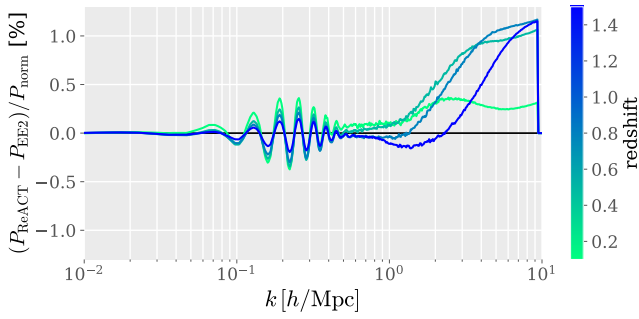


Figure 10. Effects of the matter power spectrum prescription: Normalised difference of w CDM matter power spectra produced with our standard ReACT pipeline and directly with the EE2 emulator for the same cosmological parameters. We show all the 4 redshifts considered in this work. The deviations from Λ CDM are $\{w_0, w_a\} \approx \{-0.877, -0.298\}$ for this example and no massive neutrinos or baryons are included.

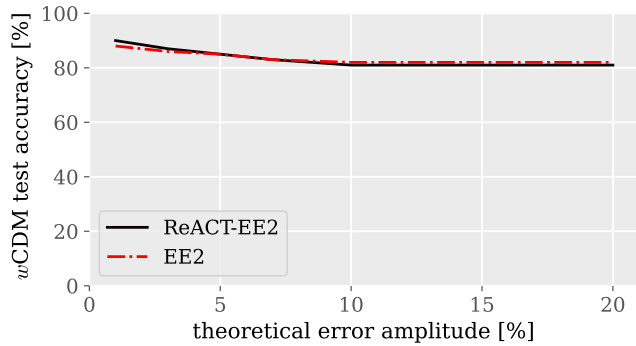


Figure 11. Effects of the matter power spectrum prescription: Test accuracies for correct class classifications when switching the w CDM test data with directly emulated w CDM spectra. The models were trained on our ReACT-EE2 test data set with various amplitudes of theory curves (20,000 training spectra per class, without massive neutrinos or baryonic feedback, $k_{\max} = 2.5 h/\text{Mpc}$). The w CDM test data is either produced with the same pipeline as the training data (ReACT-EE2) or directly emulated with EE2. The test and training data have the same cosmological parameter distributions and contain no massive neutrinos or baryonic feedback effects.

models when trained with 5% theoretical error, Figure 12 shows the total accuracy of these models for various strengths of the theoretical error.

The exclusion of smaller scales leads, in all cases, to a reduction of the total accuracy. For the EE2 test data this is of the order of ~ 2 -3%. This means that the network is able to extract information from the scales between $1.0 h/\text{Mpc}$ and $2.5 h/\text{Mpc}$ and that it is worthwhile modelling nonlinear scales. Even when we consider the lower error amplitude for a scale cut at $k_{\max} = 1.0 h/\text{Mpc}$ and compare the 4% model with the 5% of $k_{\max} = 2.5 h/\text{Mpc}$, we achieve a better accuracy going to smaller scales. The comparison of HMcode tests in Figure 12 shows that test data with a generally lower accuracy is affected even stronger by the loss of the nonlinear scales.

4.6 Priors on Cosmological Parameters

To test the effect of priors on the classification we train an EE2 network with Ω_b values from a very narrow distribution with a standard

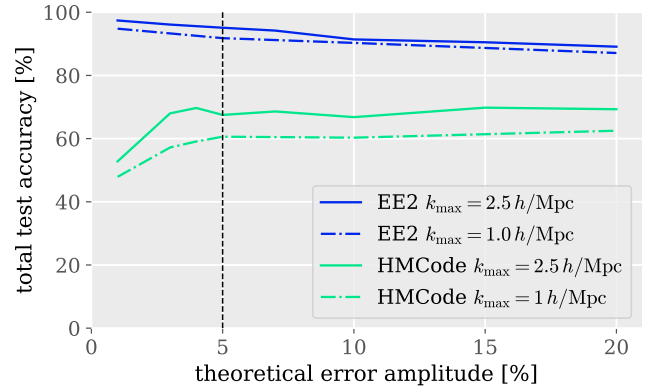


Figure 12. Influence of scale cuts: Total test accuracy of two EE2 models trained with the main EE2 training data set (20,000 training spectra per class) using scales up to $k_{\max} = 2.5 h/\text{Mpc}$ or $k_{\max} = 1.0 h/\text{Mpc}$. We show the dependence on the scaling of the theory error curves added as a noise component to the training data. All test sets have the same cosmological parameter distributions. 5% is marked as the theoretical error amplitude where the ideal theoretical error model would show convergence based on Figure 2.

deviation of 0.001 instead of 0.016. The results are shown in Figure 8. If we test this model with data based on the wider Ω_b prior then the total test accuracy gets reduced by 11%. This is an indication that the network cannot extrapolate far beyond the learned parameter range. Many spectra get instead classified as random because the random spectra are based on Λ CDM spectra with the full Ω_b parameter range. For very strong deviations from Planck’s best fit parameters it might be justified to flag them as new physics in the random class that is representing other unconsidered models. However in general, we can conclude that the influence of cosmological parameter values outside of the prior of the training data have a significant influence on the classification. Such a behaviour is not surprising and was expected both from a machine learning and cosmological perspective. This test simply warns that the prior for the training data has to be selected with care in order to maximise our confidence in the network’s predictions.

5 CONCLUSIONS

Forthcoming Stage-IV cosmological surveys will perform measurements with unprecedented accuracies, in particular at nonlinear scales. We have improved a novel machine learning approach to detect beyond-standard-model physics in the data using a Bayesian Neural Network. The purpose of this machine-learning based method is not the replacement of an MCMC analysis, but the development of a tool that can reduce the vast model space of Λ CDM modifications with high time efficiency. This includes signs for the preference of Λ CDM or hints at new physics beyond the considered cosmological classes. Once preferred models are identified, an MCMC analysis can be used to obtain parameter constraints from the selected subset. This approach reduces the data analysis time in the search for new physics without the need for biased assumptions on the model or parameter space.

Based on the halo model reaction framework, we create nonlinear dark matter power spectra for a variety of modified gravity and dark energy theories. The data shape of a matter power spectrum is chosen to roughly represent Stage IV-like survey data with four z -bins

$z \in \{1.5, 0.785, 0.478, 0.1\}$ and 100 k -bins up to $k \leq 2.5$ h/Mpc (Laureijs et al. 2011; Blanchard et al. 2020b). Our spectra include both baryonic and massive neutrino effects to increase the accuracy on nonlinear scales and enhance our ability to detect deviations from ΛCDM in an unbiased way.

Our Bayesian Cosmological Network (BaCoN-II) contains convolutional layers that perform an image analysis of the 2-dimensional matter power spectrum. It uses the information in the shape of the power spectrum to classify it into one of five classes: ΛCDM , $f(R)$, $w\text{CDM}$, DGP gravity and a ‘random’ class accounting for unknown physics. Our baseline model is able to distinguish between these classes without any major degeneracies and has a total classification accuracy of $\sim 95\%$.

The trained classification network shows a strong dependency on the choice of code for the computation of the ΛCDM spectrum. We have used direct comparisons of HMcode- and EE2-based data to investigate differences in the theoretical error and test which error model can account for this most effectively. The theory error curves developed in this work have been presented in Section 4.1. They are scaled to 5% of the normalisation spectrum to represent the error in our EE2-based data sets that has been estimated in comparison to N -body simulations. Additionally, we add Stage IV-like cosmic variance to the matter power spectrum to represent the noise in Stage-IV survey measurements.

We find that the network reaches higher classification accuracies if we include smaller scales ($k_{\text{max}} = 2.5$ h/Mpc instead of $k_{\text{max}} = 1.0$ h/Mpc), showing it is able to gain information from nonlinear scales. The baryonic feedback and massive neutrinos have a strong effect on the shape of the power spectrum, especially on nonlinear scales, but their inclusion does not reduce the classification accuracy significantly.

There are some limitations to the ability of the network to generalise: It is dependent on the choices for the parameter ranges used in the training data and has only a limited ability to extrapolate beyond these priors. This effect was to be expected and might be of use to flag strong deviations from Planck’s best fit parameters. However in general one has to be aware that the selection of priors matters. Furthermore, the influence of baryonic effects, massive neutrinos and power spectrum-specific characteristics is stronger than features generated by modified gravity and dynamic dark energy theories. This can lead to a wrong classification as ‘random’ if one of the effects is missing in the training data. Hence, a consistent construction of the random class based on accurate matter power spectrum is important. However, as the random class represents other feasible models beyond the selected ones this classification shows that BaCoN-II can successfully flag the detection of new physics.

There is a range of further improvements and new applications that we are planning for BaCoN-II. While the new theoretical error model is able to alleviate some of the systematic differences between power spectra prescriptions, it is not accounting for all of this yet. This is one indicator that it is not general enough to account for the ‘real’ systematic difference between our EE2-based prescription and the real Universe. Further refinement of the theory error curves could achieve this. They can then be used to produce random curves that do not have detectable features of the specific power spectrum prescription.

Moreover, we have seen that the network fails to classify new physics when it has not been trained with the effects of baryonic feedback. This raises the question of how different baryonic feedback models will effect the result. We also want to explore the option to constrain parameters by training a network with classes based on binning specific parameters. Lastly, with respect to the forthcoming

Stage-IV surveys, it will be necessary to move to the actual weak lensing and galaxy clustering observables for our data input, i.e., cosmic shear and redshift space galaxy spectra.

On the machine learning side, we are working on implementing explainable AI for BaCoN-II. These are methods that can explain the reasoning for a classification decision of a network to a certain extent. For example Class Activation Maps (CAMs) could find the characteristic features in a spectrum that lead to its classification as a specific modified gravity theory.

In summary, the inclusion of effects from massive neutrinos and baryonic feedback do not lead to significantly new degeneracies between the considered cosmological models. We have shown in this work that it is possible to account for large parts of the theoretical error while maintaining a high classification accuracy of $\sim 95\%$ in our 5 class model. This is a further improvement for the potential of BNNs to indicate the presence of new physics in cosmological datasets with an higher independence from theoretical limitations of the mock data production.

ACKNOWLEDGEMENTS

B.B. was supported by a UK Research and Innovation Stephen Hawking Fellowship (EP/W005654/2). A.P. is a UK Research and Innovation Future Leaders Fellow [grant MR/X005399/1]. L.T. is funded by the Science and Technology Facilities Council (STFC) and thanks the German Academic Scholarship Foundation for their support. L.L. acknowledges the support by a Swiss National Science Foundation (SNSF) Professorship grant (No. 202671). We are grateful to Joe Kennedy for his assistance and the useful discussions. We thank Michele Mancarella for the development of the BaCoN architecture. The authors thank Francesco Pace for allowing use of his modified CLASS code. We thank Ben Moews for his public python package *smurves*. For the purpose of open access, the author has applied a Creative Commons Attribution (CC BY) licence to any Author Accepted Manuscript version arising.

DATA AVAILABILITY

Alongside this paper we publish the pre-trained Bayesian Cosmological Network (BaCoN-II) which can be accessed at the github repository <https://github.com/cosmiclinux/BaCoN-II> with the training and test data available at <https://zenodo.org/records/10688282>.

REFERENCES

- Abbott B. P., et al., 2017, Gravitational Waves and Gamma-rays from a Binary Neutron Star Merger: GW170817 and GRB 170817A ([arXiv:1710.05834](https://arxiv.org/abs/1710.05834)), [doi:10.3847/2041-8213/aa920c](https://doi.org/10.3847/2041-8213/aa920c)
- Abbott T. M. C., et al., 2020, Dark Energy Survey Year 1 Results: Cosmological constraints from cluster abundances and weak lensing ([arXiv:2002.11124](https://arxiv.org/abs/2002.11124)), [doi:10.1103/PhysRevD.102.023509](https://doi.org/10.1103/PhysRevD.102.023509)
- Aghanim N., et al., 2020a, Planck 2018 results. VI. Cosmological parameters ([arXiv:1807.06209](https://arxiv.org/abs/1807.06209)), [doi:10.1051/0004-6361/201833910](https://doi.org/10.1051/0004-6361/201833910)
- Aghanim N., et al., 2020b, *A&A*, 641, A6
- Akeson R., et al., 2019, The Wide Field Infrared Survey Telescope: 100 Hubbles for the 2020s ([arXiv:1902.05569](https://arxiv.org/abs/1902.05569))
- Allen S. W., Evrard A. E., Mantz A. B., 2011, Cosmological Parameters from Observations of Galaxy Clusters ([arXiv:1103.4829](https://arxiv.org/abs/1103.4829)), [doi:10.1146/annurev-astro-081710-102514](https://doi.org/10.1146/annurev-astro-081710-102514)

- Amendola L., et al., 2018, Cosmology and fundamental physics with the Euclid satellite ([arXiv:1606.00180](#)), [doi:10.1007/s41114-017-0010-3](#)
- Anderson L., et al., 2013, *MNRAS*, 427, 3435
- Angulo R. E., Zennaro M., Contreras S., Aricò G., Pellejero-Ibañez M., Stücker J., 2020, The BACCO Simulation Project: Exploiting the full power of large-scale structure for cosmology ([arXiv:2004.06245](#))
- Angulo R. E., Zennaro M., Contreras S., Arico G., Pellejero-Ibañez M., Stücker J., 2021, The BACCO simulation project: exploiting the full power of large-scale structure for cosmology
- Aricò G., Angulo R. E., Contreras S., Ondaro-Mallea L., Pellejero-Ibañez M., Zennaro M., 2021, The BACCO simulation project: a baryonification emulator with neural networks ([arXiv:2011.15018](#)), [doi:10.1093/mnras/stab1911](#)
- Arnold C., Li B., 2019, *MNRAS*, 490, 2507
- Arnold C., Li B., Giblin B., Harnois-Déraps J., Cai Y.-C., 2021, FORGE – the $f(R)$ gravity cosmic emulator project I: Introduction and matter power spectrum emulator ([arXiv:2109.04984](#))
- Atayde L., Frusciante N., Bose B., Casas S., Barreira A., Li B., 2024, In prep.
- Baker T., Bellini E., Ferreira P. G., Lagos M., Noller J., Sawicki I., 2017, Strong constraints on cosmological gravity from GW170817 and GRB 170817A ([arXiv:1710.06394](#)), [doi:10.1103/PhysRevLett.119.251301](#)
- Battye R. A., Pace F., Trinh D., 2018, Gravitational wave constraints on dark sector models ([arXiv:1802.09447](#)), [doi:10.1103/PhysRevD.98.023504](#)
- Bernardo H., Bose B., Franzmann G., Hagstotz S., He Y., Litsa A., Niedermann F., 2023, *Universe*, 9, 63
- Beutler F., et al., 2017, *MNRAS*, 466, 2242
- Bird S., Viel M., Haehnelt M. G., 2012, Massive neutrinos and the non-linear matter power spectrum ([arXiv:1109.4416](#)), [doi:10.1111/j.1365-2966.2011.20222.x](#)
- Bird S., Ali-Haïmoud Y., Feng Y., Liu J., 2018, An efficient and accurate hybrid method for simulating non-linear neutrino structure ([arXiv:1803.09854](#)), [doi:10.1093/mnras/sty2376](#)
- Blanchard A., et al., 2020a, Euclid preparation: VII. Forecast validation for Euclid cosmological probes ([arXiv:1910.09273](#)), [doi:10.1051/0004-6361/202038071](#)
- Blanchard A., et al., 2020b, *A&A*, 642, A191
- Blas D., Lesgourgues J., Tram T., 2011, *JCAP*, 07, 034
- Blas D., Garny M., Konstandin T., Lesgourgues J., 2014, Structure formation with massive neutrinos: going beyond linear theory ([arXiv:1408.2995](#)), [doi:10.1088/1475-7516/2014/11/039](#)
- Blundell C., Cornebise J., Kavukcuoglu K., Wierstra D., 2015, in International conference on machine learning. pp 1613–1622
- Bose B., Cataneo M., Tröster T., Xia Q., Heymans C., Lombriser L., 2020, On the road to per cent accuracy IV: ReACT – computing the non-linear power spectrum beyond Λ CDM ([arXiv:2005.12184](#)), [doi:10.1093/mnras/staa2696](#)
- Bose B., et al., 2021, On the road to per cent accuracy – V. The non-linear power spectrum beyond Λ CDM with massive neutrinos and baryonic feedback ([arXiv:2105.12114](#)), [doi:10.1093/mnras/stab2731](#)
- Bose B., Tsedrik M., Kennedy J., Lombriser L., Pourtsidou A., Taylor A., 2022, Fast and accurate predictions of the nonlinear matter power spectrum for general models of Dark Energy and Modified Gravity ([arXiv:2210.01094](#)), [doi:10.1093/mnras/stac3783](#)
- Brax P., Valageas P., 2017, Goldstone models of modified gravity ([arXiv:1611.08279](#)), [doi:10.1103/PhysRevD.95.043515](#)
- Brax P., Casas S., Desmond H., Elder B., 2021, *Universe*, 8, 11
- Burgess C. P., 2004, Towards a natural theory of dark energy: Supersymmetric large extra dimensions ([arXiv:hep-th/0411140](#)), [doi:10.1063/1.1848343](#)
- Burrage C., 2019, What laboratory experiments can teach us about cosmology: A chameleon example ([arXiv:1901.01784](#)), [doi:10.1051/epjconf/201921905001](#)
- Carrion K., Carrillo P., Spurio Mancini A., Pourtsidou A., Hidalgo J. C., 2024, Dark Scattering: accelerated constraints from KiDS-1000 with ReACT and CosmoPower ([arXiv:2402.18562](#))
- Cataneo M., Lombriser L., Heymans C., Mead A., Barreira A., Bose S., Li B., 2019, On the road to per cent accuracy: non-linear reaction of the matter power spectrum to dark energy and modified gravity ([arXiv:1812.05594](#)), [doi:10.1093/mnras/stz1836](#)
- Cataneo M., Emberson J. D., Inman D., Harnois-Déraps J., Heymans C., 2020, On the road to per cent accuracy – III. Non-linear reaction of the matter power spectrum to massive neutrinos ([arXiv:1909.02561](#)), [doi:10.1093/mnras/stz3189](#)
- Charnock T., Perreault-Levasseur L., Lanusse F., 2022, in , Artificial Intelligence for High Energy Physics. World Scientific, pp 663–713
- Chevallier M., Polarski D., 2001, *Int. J. Mod. Phys. D*, 10, 213
- Chisari N. E., et al., 2019, Modelling baryonic feedback for survey cosmology ([arXiv:1905.06082](#)), [doi:10.21105/astro.1905.06082](#)
- Clifton T., Ferreira P. G., Padilla A., Skordis C., 2012, *Physics Reports*, 513, 1
- Clowe D., Bradac M., Gonzalez A. H., Markevitch M., Randall S. W., Jones C., Zaritsky D., 2006, A direct empirical proof of the existence of dark matter ([arXiv:astro-ph/0608407](#)), [doi:10.1086/508162](#)
- Copland E. J., Sami M., Tsujikawa S., 2006, *Int. J. Mod. Phys. D*, 15, 1753
- Corbelli E., Salucci P., 2000, The Extended Rotation Curve and the Dark Matter Halo of M33 ([arXiv:astro-ph/9909252](#)), [doi:10.1046/j.1365-8711.2000.03075.x](#)
- Creminelli P., Vernizzi F., 2017, Dark Energy after GW170817 and GRB170817A ([arXiv:1710.05877](#)), [doi:10.1103/PhysRevLett.119.251302](#)
- Creminelli P., Lewandowski M., Tambalo G., Vernizzi F., 2018, Gravitational Wave Decay into Dark Energy ([arXiv:1809.03484](#)), [doi:10.1088/1475-7516/2018/12/025](#)
- Donald-McCann J., Beutler F., Koyama K., Karamanis M., 2021, matryoshka: Halo Model Emulator for the Galaxy Power Spectrum ([arXiv:2109.15236](#))
- Dvali G. R., Gabadadze G., Porrati M., 2000, 4-D gravity on a brane in 5-D Minkowski space ([arXiv:hep-th/0005016](#)), [doi:10.1016/S0370-2693\(00\)00669-9](#)
- Esteban I., Gonzalez-Garcia M. C., Maltoni M., Schwetz T., Zhou A., 2020, *JHEP*, 09, 178
- Ezquiaga J. M., Zumalacárregui M., 2017, Dark Energy After GW170817: Dead Ends and the Road Ahead ([arXiv:1710.05901](#)), [doi:10.1103/PhysRevLett.119.251304](#)
- Frusciante N., et al., 2023, Euclid: Constraining linearly scale-independent modifications of gravity with the spectroscopic and photometric primary probes ([arXiv:2306.12368](#))
- Gal Y., Ghahramani Z., 2016, in international conference on machine learning. pp 1050–1059 ([arXiv:1506.02142](#))
- Gatti M., et al., 2021, Dark Energy Survey Year 3 results: cosmology with moments of weak lensing mass maps ([arXiv:2110.10141](#))
- Giri S. K., Schneider A., 2021, *JCAP*, 12, 046
- Gubitosi G., Piazza F., Vernizzi F., 2013, The Effective Field Theory of Dark Energy ([arXiv:1210.0201](#)), [doi:10.1088/1475-7516/2013/02/032](#)
- Heymans C., et al., 2021, KiDS-1000 Cosmology: Multi-probe weak gravitational lensing and spectroscopic galaxy clustering constraints ([arXiv:2007.15632](#)), [doi:10.1051/0004-6361/202039063](#)
- Hildebrandt H., et al., 2017, *MNRAS*, 465, 1454
- Hu W., Sawicki I., 2007, *Phys. Rev. D*, 76, 064004
- Huterer D., Shafer D. L., 2018, Dark energy two decades after: Observables, probes, consistency tests ([arXiv:1709.01091](#)), [doi:10.1088/1361-6633/aa997e](#)
- Islam M. A., Jia S., Bruce N. D., 2019, in International Conference on Learning Representations.
- Khoury J., Weltman A., 2004, *Phys. Rev. D*, 69, 044026
- Knabenhans M., et al., 2021, Euclid preparation: IX. EuclidEmulator2 – power spectrum emulation with massive neutrinos and self-consistent dark energy perturbations ([arXiv:2010.11288](#)), [doi:10.1093/mnras/stab1366](#)
- Kobayashi Y., Nishimichi T., Takada M., Takahashi R., Osato K., 2020, Accurate emulator for the redshift-space power spectrum of dark matter halos and its application to galaxy power spectrum ([arXiv:2005.06122](#)), [doi:10.1103/PhysRevD.102.063504](#)
- Koyama K., 2016, Cosmological Tests of Modified Gravity ([arXiv:1504.04623](#)), [doi:10.1088/0034-4885/79/4/046902](#)
- LSST Dark Energy Science Collaboration 2012, Large Synoptic Survey Tele-

- scope: Dark Energy Science Collaboration ([arXiv:1211.0310](https://arxiv.org/abs/1211.0310))
- Lawrence E., et al., 2011, [arXiv e-prints](https://arxiv.org/abs/1110.3193), p. [arXiv:1110.3193](https://arxiv.org/abs/1110.3193)
- Lawrence E., et al., 2017, The Mira-Titan Universe. II. Matter Power Spectrum Emulation ([arXiv:1705.03388](https://arxiv.org/abs/1705.03388)), [doi:10.3847/1538-4357/aa86a9](https://doi.org/10.3847/1538-4357/aa86a9)
- LeCun Y., Bengio Y., Hinton G., 2015, Deep learning, [doi:10.1038/nature14539](https://doi.org/10.1038/nature14539), <https://doi.org/10.1038/nature14539>
- Lesgourgues J., 2011, The Cosmic Linear Anisotropy Solving System (CLASS) I: Overview ([arXiv:1104.2932](https://arxiv.org/abs/1104.2932))
- Levi M., et al., 2019, in Bulletin of the American Astronomical Society. p. 57 ([arXiv:1907.10688](https://arxiv.org/abs/1907.10688))
- Lin H. W., Tegmark M., Rolnick D., 2017, Why Does Deep and Cheap Learning Work So Well?, [doi:10.1007/s10955-017-1836-5](https://doi.org/10.1007/s10955-017-1836-5), <https://doi.org/10.1007/s10955-017-1836-5>
- Linder E. V., 2003, *Phys. Rev. Lett.*, 90, 091301
- Lombriser L., Lima N. A., 2017, Challenges to Self-Acceleration in Modified Gravity from Gravitational Waves and Large-Scale Structure ([arXiv:1602.07670](https://arxiv.org/abs/1602.07670)), [doi:10.1016/j.physletb.2016.12.048](https://doi.org/10.1016/j.physletb.2016.12.048)
- Lombriser L., Taylor A., 2016, Breaking a Dark Degeneracy with Gravitational Waves ([arXiv:1509.08458](https://arxiv.org/abs/1509.08458)), [doi:10.1088/1475-7516/2016/03/031](https://doi.org/10.1088/1475-7516/2016/03/031)
- MacKay D. J. C., 1992, *Neural Computation*, 4, 448
- Mancarella M., Kennedy J., Bose B., Lombriser L., 2020, Seeking New Physics in Cosmology with Bayesian Neural Networks I: Dark Energy and Modified Gravity ([arXiv:2012.03992](https://arxiv.org/abs/2012.03992))
- Martinelli M., et al., 2021, *A&A*, 649, A100
- Massara E., Villaescusa-Navarro F., Viel M., 2014, The halo model in a massive neutrino cosmology ([arXiv:1410.6813](https://arxiv.org/abs/1410.6813)), [doi:10.1088/1475-7516/2014/12/053](https://doi.org/10.1088/1475-7516/2014/12/053)
- McCarthy I. G., Schaye J., Bird S., Le Brun A. M. C., 2017, *MNRAS*, 465, 2936
- Mead A., Peacock J., Heymans C., Joudaki S., Heavens A., 2015, *MNRAS*, 454, 1958
- Mead A. J., Heymans C., Lombriser L., Peacock J. A., Steele O. I., Winther H. A., 2016a, Accurate halo-model matter power spectra with dark energy, massive neutrinos and modified gravitational forces ([arXiv:1602.02154](https://arxiv.org/abs/1602.02154)), [doi:10.1093/mnras/stw681](https://doi.org/10.1093/mnras/stw681)
- Mead A., Heymans C., Lombriser L., Peacock J., Steele O., Winther H., 2016b, Accurate halo-model matter power spectra with dark energy, massive neutrinos and modified gravitational forces ([arXiv:1602.02154](https://arxiv.org/abs/1602.02154)), [doi:10.1093/mnras/stw681](https://doi.org/10.1093/mnras/stw681)
- Mead A., Brieden S., Tröster T., Heymans C., 2020, HMcode-2020: Improved modelling of non-linear cosmological power spectra with baryonic feedback ([arXiv:2009.01858](https://arxiv.org/abs/2009.01858)), [doi:10.1093/mnras/stab082](https://doi.org/10.1093/mnras/stab082)
- Mehta P., Bukov M., Wang C.-H., Day A. r. G. R., Richardson C., Fisher C. K., Schwab D. J., 2019, A high-bias, low-variance introduction to Machine Learning for physicists ([arXiv:1803.08823](https://arxiv.org/abs/1803.08823)), [doi:10.1016/j.physrep.2019.03.001](https://doi.org/10.1016/j.physrep.2019.03.001)
- Moews B., et al., 2019, *Physical Review D*, 99, 123529
- Mummery B. O., McCarthy I. G., Bird S., Schaye J., 2017, The separate and combined effects of baryon physics and neutrino free streaming on large-scale structure ([arXiv:1702.02064](https://arxiv.org/abs/1702.02064)), [doi:10.1093/mnras/stx1469](https://doi.org/10.1093/mnras/stx1469)
- Neal R. M., 1996, *Bayesian Learning for Neural Networks*. Springer-Verlag, Berlin, Heidelberg
- Nishimichi T., et al., 2019, Dark Quest. I. Fast and Accurate Emulation of Halo Clustering Statistics and Its Application to Galaxy Clustering ([arXiv:1811.09504](https://arxiv.org/abs/1811.09504)), [doi:10.3847/1538-4357/ab3719](https://doi.org/10.3847/1538-4357/ab3719)
- Noller J., 2020, Cosmological constraints on dark energy in light of gravitational wave bounds ([arXiv:2001.05469](https://arxiv.org/abs/2001.05469)), [doi:10.1103/PhysRevD.101.063524](https://doi.org/10.1103/PhysRevD.101.063524)
- Paribelli G., Carbone C., Bel J., Bose B., Calabrese M., Carella E., Zennaro M., 2022, *JCAP*, 11, 041
- Perenon L., Bel J., Maartens R., de la Cruz-Dombriz A., 2019, Optimising growth of structure constraints on modified gravity ([arXiv:1901.11063](https://arxiv.org/abs/1901.11063)), [doi:10.1088/1475-7516/2019/06/020](https://doi.org/10.1088/1475-7516/2019/06/020)
- Ramachandra N., Valogiannis G., Ishak M., Heitmann K., 2021, Matter Power Spectrum Emulator for f(R) Modified Gravity Cosmologies ([arXiv:2010.00596](https://arxiv.org/abs/2010.00596)), [doi:10.1103/PhysRevD.103.123525](https://doi.org/10.1103/PhysRevD.103.123525)
- Sakstein J., Jain B., 2017, Implications of the Neutron Star Merger GW170817 for Cosmological Scalar-Tensor Theories ([arXiv:1710.05893](https://arxiv.org/abs/1710.05893)), [doi:10.1103/PhysRevLett.119.251303](https://doi.org/10.1103/PhysRevLett.119.251303)
- Salvatelli V., Piazza F., Marinoni C., 2016, Constraints on modified gravity from Planck 2015: when the health of your theory makes the difference ([arXiv:1602.08283](https://arxiv.org/abs/1602.08283)), [doi:10.1088/1475-7516/2016/09/027](https://doi.org/10.1088/1475-7516/2016/09/027)
- Schneider A., Teyssier R., Stadel J., Chisari N. E., Le Brun A. M. C., Amara A., Refregier A., 2019, Quantifying baryon effects on the matter power spectrum and the weak lensing shear correlation ([arXiv:1810.08629](https://arxiv.org/abs/1810.08629)), [doi:10.1088/1475-7516/2019/03/020](https://doi.org/10.1088/1475-7516/2019/03/020)
- Schneider A., Stoira N., Refregier A., Weiss A. J., Knabenhans M., Stadel J., Teyssier R., 2020a, Baryonic effects for weak lensing. Part I. Power spectrum and covariance matrix ([arXiv:1910.11357](https://arxiv.org/abs/1910.11357)), [doi:10.1088/1475-7516/2020/04/019](https://doi.org/10.1088/1475-7516/2020/04/019)
- Schneider A., et al., 2020b, Baryonic effects for weak lensing. Part II. Combination with X-ray data and extended cosmologies ([arXiv:1911.08494](https://arxiv.org/abs/1911.08494)), [doi:10.1088/1475-7516/2020/04/020](https://doi.org/10.1088/1475-7516/2020/04/020)
- Semboloni E., Hoekstra H., Schaye J., van Daalen M. P., McCarthy I. J., 2011, *MNRAS*, 417, 2020
- Song Y.-S., et al., 2015, *Phys. Rev.*, D92, 043522
- Springel V., et al., 2018, First results from the IllustrisTNG simulations: matter and galaxy clustering ([arXiv:1707.03397](https://arxiv.org/abs/1707.03397)), [doi:10.1093/mnras/stx3304](https://doi.org/10.1093/mnras/stx3304)
- Spurio Mancini A., Bose B., 2023, On the degeneracies between baryons, massive neutrinos and f(R) gravity in Stage IV cosmic shear analyses ([arXiv:2305.06350](https://arxiv.org/abs/2305.06350)), [doi:10.21105/astro.2305.06350](https://doi.org/10.21105/astro.2305.06350)
- Takahashi R., Sato M., Nishimichi T., Taruya A., Oguri M., 2012, *Astrophys. J.*, 761, 152
- Tram T., Brandbyge J., Dakin J., Hannestad S., 2019, Fully relativistic treatment of light neutrinos in N -body simulations ([arXiv:1811.00904](https://arxiv.org/abs/1811.00904)), [doi:10.1088/1475-7516/2019/03/022](https://doi.org/10.1088/1475-7516/2019/03/022)
- Tröster T., et al., 2021, *A&A*, 649, A88
- Tsedrik M., Bose B., Carrilho P., Pourtsidou A., Pamuk S., Casas S., Lesgourgues J., 2024, In prep.
- Vainshtein A. I., 1972, *Phys. Lett. B*, 39, 393
- Valentin Jospin L., Buntine W., Boussaïd F., Laga H., Bennamoun M., 2020, *arXiv e-prints*,
- Will C. M., 2014, The Confrontation between General Relativity and Experiment ([arXiv:1403.7377](https://arxiv.org/abs/1403.7377)), [doi:10.12942/lrr-2014-4](https://doi.org/10.12942/lrr-2014-4)
- Winther H., Casas S., Baldi M., Koyama K., Li B., Lombriser L., Zhao G.-B., 2019, Emulators for the nonlinear matter power spectrum beyond Λ CDM ([arXiv:1903.08798](https://arxiv.org/abs/1903.08798)), [doi:10.1103/PhysRevD.100.123540](https://doi.org/10.1103/PhysRevD.100.123540)
- Wright B. S., Winther H. A., Koyama K., 2017, COLA with massive neutrinos ([arXiv:1705.08165](https://arxiv.org/abs/1705.08165)), [doi:10.1088/1475-7516/2017/10/054](https://doi.org/10.1088/1475-7516/2017/10/054)
- Wright B. S., Koyama K., Winther H. A., Zhao G.-B., 2019, Investigating the degeneracy between modified gravity and massive neutrinos with redshift-space distortions ([arXiv:1902.10692](https://arxiv.org/abs/1902.10692)), [doi:10.1088/1475-7516/2019/06/040](https://doi.org/10.1088/1475-7516/2019/06/040)
- Zhong X., Gallagher B., Liu S., Kaikhura B., Hiszpanski A., Han T. Y.-J., 2022, *npj Computational Materials*, 8, 204
- Zhou B., Khosla A., Lapedriza A., Oliva A., Torralba A., 2016, in Proceedings of the IEEE conference on computer vision and pattern recognition. pp 2921–2929
- de Rham C., Melville S., 2018, Gravitational Rainbows: LIGO and Dark Energy at its Cutoff ([arXiv:1806.09417](https://arxiv.org/abs/1806.09417)), [doi:10.1103/PhysRevLett.121.221101](https://doi.org/10.1103/PhysRevLett.121.221101)
- van Daalen M. P., Schaye J., Booth C. M., Dalla Vecchia C., 2011, The effects of galaxy formation on the matter power spectrum: a challenge for precision cosmology ([arXiv:1104.1174](https://arxiv.org/abs/1104.1174)), [doi:10.1111/j.1365-2966.2011.18981.x](https://doi.org/10.1111/j.1365-2966.2011.18981.x)
- van Daalen M. P., McCarthy I. G., Schaye J., 2020, Exploring the effects of galaxy formation on matter clustering through a library of simulation power spectra ([arXiv:1906.00968](https://arxiv.org/abs/1906.00968)), [doi:10.1093/mnras/stz3199](https://doi.org/10.1093/mnras/stz3199)

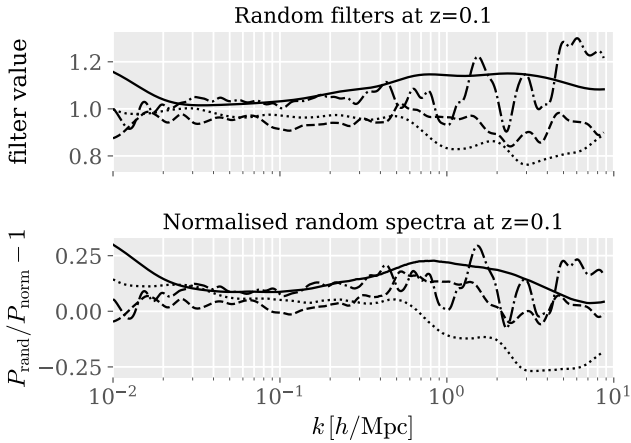


Figure A1. Four different random filters are shown for $z = 0.1$ in the upper panel. They are then each multiplied with a randomly drawn Λ CDM spectrum to produce a random spectrum. These are shown in the lower panel after being normalised with the Planck Λ CDM spectrum.

APPENDIX A: RANDOM SPECTRA

The random class represents models that are currently unknown. It was added to identify a cosmology which is not amongst our selected classes instead of wrongly classifying it as one of them. It is not actually completely random but instead contains features that other feasible models might introduce in the power spectrum. We create the random class by combining a Λ CDM matter power spectrum with random filters. The random filters should contain signatures that are k and z correlated to mimic real physical models and an algorithm to produce these was presented in [Mancarella et al. \(2020\)](#). We have updated these filters since our last work to account for more realistic and subtle deviations from currently known theories. This was done by including wider variances in the correlation length in both k and z as well as reducing the fluctuations allowed at large scales. A set of four filters with randomly generated features that are correlated in k and z is shown at the top of [Figure A1](#). The bottom panel shows spectra of yet unknown physics after the filters have been multiplied with randomly selected Λ CDM spectra. We have seen in [Section 4](#) that it is important to build the random class from spectra that include effects of known physics like baryonic feedback and then use the random filters to account for unknown physics on top of that. For this reason we base them on Λ CDM spectra from the most accurate EE2 training and test data set with massive neutrinos and baryonic feedback. The Mathematica notebook including the algorithm is available [here](#).

APPENDIX B: PARAMETER EFFECTS ON THE POWER SPECTRUM

This section visualises the effects of model parameters for dynamical dark energy and modified gravity as well as the sum of neutrino masses and the strength of baryonic feedback on the matter power spectrum. [Figure B1](#) shows the characteristic changes when one parameter is varied while the other cosmological parameters are fixed to the Planck best-fit values (see [Table 1](#)). The plotted values are representative of the prior ranges described in [Section 2.3](#). The selected classes show different characteristic influences on the power spectrum. Stronger modifications of DGP lead to increased ampli-

tudes of the power spectrum on large scales while $f(R)$ introduces a strong scale dependence on small scales. Baryonic feedback has a very strong influence on nonlinear scales while the neutrino mass also affects BAO-scales. These specific features allow the network to distinguish the different cosmological classes even when the cosmological parameters are varied. Some of the curves show a small spike which is an artefact from the ReACT computation. These numerical glitches are above the scales we consider so they do not affect our results.

This paper has been typeset from a $\text{\TeX}/\text{\LaTeX}$ file prepared by the author.

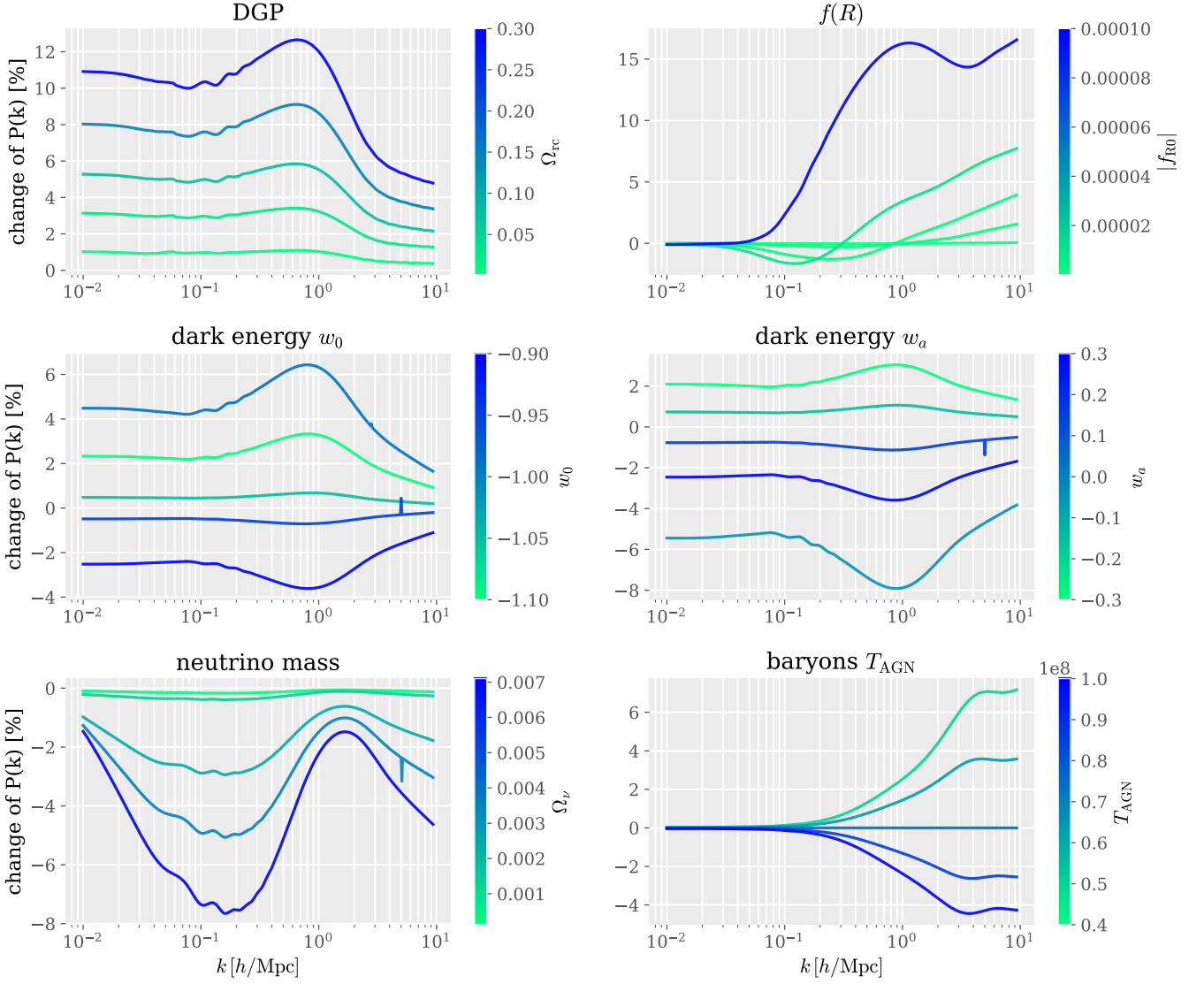


Figure B1. Influence of cosmological model parameters on the power spectrum. Other cosmological parameters are fixed to the mean values given in Table 1. We normalise the spectra by the Planck ΛCDM spectrum without massive neutrinos but with baryonic feedback assuming $T_{\text{AGN}} = 6.3 \times 10^7$ K. All values are within the prior ranges of the training data.